



HAL
open science

One-helix protein 2 is not required for the synthesis of photosystem II subunit D1 in *Chlamydomonas*

Fei Wang, Korbinian Dischinger, Lisa Désirée Westrich, Irene Meindl, Felix Egidi, Raphael Trösch, Frederik Sommer, Xenie Johnson, Michael Schroda, Joerg Nickelsen, et al.

► **To cite this version:**

Fei Wang, Korbinian Dischinger, Lisa Désirée Westrich, Irene Meindl, Felix Egidi, et al.. One-helix protein 2 is not required for the synthesis of photosystem II subunit D1 in *Chlamydomonas*. *Plant Physiology*, 2023, 191 (3), pp.1612-1633. 10.1093/plphys/kiad015 . hal-04337791

HAL Id: hal-04337791

<https://hal.science/hal-04337791>

Submitted on 13 Dec 2023

HAL is a multi-disciplinary open access archive for the deposit and dissemination of scientific research documents, whether they are published or not. The documents may come from teaching and research institutions in France or abroad, or from public or private research centers.

L'archive ouverte pluridisciplinaire **HAL**, est destinée au dépôt et à la diffusion de documents scientifiques de niveau recherche, publiés ou non, émanant des établissements d'enseignement et de recherche français ou étrangers, des laboratoires publics ou privés.

One-helix protein 2 is not required for the synthesis of photosystem II subunit

D1 in *Chlamydomonas*

3

4 Fei Wang^{1,4,5}, Korbinian Dischinger¹, Lisa Désirée Westrich², Irene Meindl¹, Felix
5 Egidi¹, Raphael Trösch², Frederik Sommer³, Xenie Johnson^{4,6}, Michael Schroda³,
6 Joerg Nickelsen¹, Felix Willmund², Olivier Vallon^{4,*}, Alexandra-Viola Bohne^{1,*}

7

8 ¹Molecular Plant Sciences, LMU Munich, Planegg-Martinsried, 82152, Germany

9 ²Molecular Genetics of Eukaryotes, University of Kaiserslautern, 67663
10 Kaiserslautern, Germany

11 ³Molecular Biotechnology & Systems Biology, University of Kaiserslautern, 67663
12 Kaiserslautern, Germany

13 ⁴UMR 7141, Centre National de la Recherche Scientifique/Sorbonne Université,
14 Institut de Biologie Physico-Chimique, Paris 75005, France

15 ⁵College of Life Sciences, Northwest University, Xi'an 710069, China

16

17 ⁶Present address: CEA, BIAM, Aix-Marseille Université, Saint-Paul-lez-Durance, F-
18 13108, France

19

20 *Contact information: Olivier Vallon (ovallon@ibpc.fr) and Alexandra-Viola Bohne
21 (alexandra.bohne@lmu.de)

22

23 **RUNNING TITLE**

24 D1 synthesis uncoupled from cofactor assembly

25

26 **ABSTRACT**

27 In land plants, co-translational association of chlorophyll (Chl) to the nascent D1
28 polypeptide, a reaction center protein of photosystem II (PSII), requires a Chl binding
29 complex consisting of HCF244 and two conserved One-Helix Proteins, OHP1 and
30 OHP2. Here, we show that an *ohp2* mutant of the green alga *Chlamydomonas*
31 *reinhardtii* fails to accumulate core PSII subunits, in particular D1. Extragenic
32 suppressors arise at high frequency, suggesting the existence of another route for

33 Chl association to PSII. The *ohp2* mutant can be complemented by the *Arabidopsis*
34 ortholog. In contrast to land plants, where translation is halted in the absence of
35 OHP2, pulse labelling and ribosome profiling experiments show that the
36 *Chlamydomonas* mutant translates the *psbA* transcript over its full length, and D1 is
37 degraded during or immediately after translation. The translation of other PSII
38 subunits is affected by assembly-controlled translational regulation (the CES
39 process). Proteomics shows that the OHP2 complex partner HCF244 still partly
40 accumulates in *ohp2*. This contrasts with the situation in land plants and explains the
41 persistence of *psbA* translation in the *Chlamydomonas* mutant. Several Chl
42 biosynthesis enzymes overaccumulate in the mutant membranes. Partial inactivation
43 of the D1-degrading FtsH protease restores a low level of PSII activity in an *ohp2*
44 background, but not photoautotrophy. Taken together, our data suggest that OHP2 is
45 involved in establishing a proper conformation and/or cofactor association to newly
46 synthesized D1, such that its absence leads to rapid degradation of D1. However, the
47 OHP2 complex is not required for *psbA* translation in *Chlamydomonas*.

48

49

50 **KEYWORDS**

51 One-Helix Protein; photosystem II; light harvesting-like family; D1 protein; *psbA*
52 mRNA; ribosome profiling; targeted proteomics; control by epistasy of synthesis;
53 cross-species complementation; FtsH protease

54 INTRODUCTION

55 Oxygenic photosynthesis, carried out by cyanobacteria and photosynthetic
56 eukaryotes, is based on the light-driven electron transfer from water to NADPH,
57 involving three complexes located in the thylakoid membrane and operating in series:
58 photosystem II (PSII), cytochrome *b₆f* (*Cytb₆f*) and photosystem I (PSI). Electron
59 transfer generates a proton gradient across the membrane, which allows production
60 of ATP by the ATP synthase, thus fueling CO₂ fixation. PSII is a multi-subunit
61 complex. Depending on the organism, its core complex is made up of 20-23 subunits:
62 the reaction center proteins D1 (PsbA), D2 (PsbD), *Cytb₅₅₉* (subunits PsbE and
63 PsbF) and PsbI are encoded in the chloroplast genome by the *psbA*, *psbD*, *psbE/F*
64 and *psbI* genes, as are the core antenna CP47 (PsbB) and CP43 (PsbC) and the
65 additional subunits PsbH, PsbJ, PsbK, PsbL, PsbM, PsbT and PsbZ (reviewed in e.g.
66 Gao et al., 2018). In eukaryotes, nucleus-encoded subunits complete the complex
67 and build its peripheral chlorophyll (Chl) *a/b* containing light-harvesting antenna
68 complexes (LHCs). Chl *a* and its derivative pheophytin (Phe) *a* are essential
69 components of the intra-PSII electron transfer chain that allows the generation of a
70 stable charge separated state after light-capture, formed between the special pair
71 P680⁺ and the plastoquinone Q_A⁻. The redox-active cofactors are scaffolded mainly
72 by the homologous D1 and D2 polypeptides, which also provide Tyr residues
73 involved in re-reduction of P680⁺ and residues liganding the manganese (Mn)-cluster
74 where water-splitting occurs. Given the tight folding of the enzyme and the high
75 chemical reactivity of Chl cation radicals that can form from the light-excited states, it
76 has long been hypothesized that specific mechanisms must coordinate the synthesis
77 of the reaction center proteins, their intra-membrane insertion and their association
78 with pigments. Over the years, the biogenesis of PSII has been dissected into a
79 series of discrete assembly steps (reviewed in Nickelsen and Rengstl, 2013).
80 Precursor D1 (pD1) is co-translationally inserted into the membrane, binds to PsbI
81 and interacts with a complex formed between *Cytb₅₅₉* and D2 to build the reaction
82 center (RC) subcomplex. Successive integration of CP47, then CP43, associated
83 with other small subunits, forms the monomeric PSII core. Dimerization ensues, as
84 well as association with LHCs imported from the cytosol. On the luminal surface of
85 the enzyme, cleavage of the C-terminal extension of pD1 and light-driven assembly
86 of the Mn-containing cluster allow formation of the water-splitting enzyme.

87 Over the years, numerous proteins have been found to catalyze various steps of
88 the PSII assembly pathway, both during *de novo* assembly and during repair after
89 photoinhibition (Heinz et al., 2016; Lu, 2016). Some act by regulating gene
90 expression, in particular translation of *psbA* which codes for the rapidly-turning over
91 D1. Others act as a chaperone, binding an assembly intermediate until the next step
92 can be completed. In this category, particular attention has been paid to proteins that
93 could mediate the assembly of the cofactors. In the final PSII structure, the numerous
94 cofactors (Chl, Phe, carotenoids (Car), Fe, the Mn_4CaO_5 cluster) are held in a very
95 precise location by virtue of their interaction with specific amino acids of the tightly
96 packed polypeptide chains. How this organization is achieved during a progressive
97 assembly pipeline remains largely a mystery. Chl molecules are of particular interest
98 because of the high chemical reactivity of their excited states. It is believed that they
99 are presented to the acceptor PSII subunits by specific carrier proteins that precisely
100 mediate their insertion at the proper position, at the proper stage of assembly. In
101 *Arabidopsis*, a complex consisting of two conserved One-Helix Proteins, OHP1 and
102 OHP2, and a protein related to short-chain dehydrogenase/reductases, HCF244, has
103 been found to be essential for Chl integration into PSII, or for protection of the newly
104 synthesized Chl-associated D1 during formation of the RC complex (Chotewutmontri
105 and Barkan, 2020; Chotewutmontri et al., 2020; Hey and Grimm, 2018; Li et al.,
106 2019; Myouga et al., 2018). In combination with OHP1, OHP2 is able to bind Car and
107 Chl, the latter via specific residues of a Chl binding motif (Hey and Grimm, 2020), and
108 this heterodimer has unique photoprotective properties (Psencik et al., 2020). The
109 **OHP1/OHP2/HCF244 Complex** (which we will hereafter call "OHC") is homologous to
110 a complex of similar function described in cyanobacteria. OHP1 and OHP2, although
111 they belong to two distinct clades of the light-harvesting superfamily, resemble
112 cyanobacterial High Light-Inducible Proteins (HLIPs) encoded by the *hliA-D* genes
113 which also harbor a single transmembrane domain showing the key residues for
114 binding Chl (Engelken et al., 2010). HliC and HliD have been found, together with the
115 HCF244 homolog Ycf39, to associate with the RC subcomplex (Chidgey et al., 2014;
116 Knoppová et al., 2014) and HliD can bind Chl and β -carotene (Staleva et al., 2015).
117 The Chl synthase ChlG co-immunoprecipitates with HliD/Ycf39 and it is believed that
118 the complex can deliver newly synthesized Chl to D1 and/or D2 during or early after
119 their translation (Chidgey et al., 2014; Staleva et al., 2015). For this process, Chl
120 could also be scavenged from other Chl-binding proteins upon their degradation.

121 The phenotype of land plant mutants has revealed an additional function of the
122 OHC, namely to regulate *psbA* translation. *Arabidopsis ohp1*, *ohp2* and *hcf244*
123 mutants show strongly reduced PSII levels, while only weak or indirect effects are
124 observed on PSI accumulation (Beck et al., 2017; Li et al., 2019; Link et al., 2012;
125 Myouga et al., 2018). In the three mutants, the other two partners of the OHC are
126 dramatically reduced, suggesting that formation of the complex is required for their
127 stabilization (Beck et al., 2017; Hey and Grimm, 2020; Li et al., 2019). Interestingly,
128 *ohp1* and *ohp2* mutants from *Arabidopsis* as well as an *hcf244* mutant from maize
129 show a near complete inhibition of *psbA* translation, as judged by the very sensitive
130 assay of ribosome footprint sequencing (RF-Seq; Chotewutmontri et al., 2020). This
131 has led to the hypothesis that the OHC regulates *psbA* translation by sensing the
132 production of D1 properly loaded with Chl: as long as D1 remains bound to the OHC,
133 the complex is unable to catalyze *psbA* translation initiation and D1 translation is
134 halted (Chotewutmontri and Barkan, 2020). Such a tight coupling between assembly
135 and translation is reminiscent of a process described as Control by Epistasy of
136 Synthesis (CES) in *Chlamydomonas* (Minai et al., 2006; Wollman et al., 1999). In the
137 PSII CES cascade, unassembled D1, as produced for example in the absence of D2,
138 represses its own translation initiation. It was thus of particular interest to determine
139 whether an OHC exists in *Chlamydomonas* and plays a similar role as in
140 *Synechocystis* or *Arabidopsis*.

141 Many other proteins of the PSII assembly pathway appear conserved between
142 cyanobacteria, land plants and *Chlamydomonas*, but their detailed working
143 mechanism has only rarely been investigated in the alga (Spaniol et al., 2021).
144 Among those acting at a site close to that of the OHC, another short-chain
145 dehydrogenase/reductase, HCF173, has been found to be necessary for D1
146 translation and to bind the *psbA* 5' UTR, along with another protein of ill-defined
147 function, SRRP1 (Link et al., 2012; McDermott et al., 2019; Schult et al., 2007;
148 Watkins et al., 2020). ALB3, which belongs to a conserved family of protein
149 integrases also found in bacteria and mitochondria, plays a major role in the insertion
150 of integral thylakoid membrane proteins in general, and serves as a hub for many
151 other factors (reviewed in Plöschinger et al., 2016). In the case of D1, ALB3 appears
152 to interact with factors acting downstream of D1 integration, namely HCF136, but
153 also LPA1 and probably LPA2 and LPA3. HCF136 (and its homolog Ycf48 in
154 cyanobacteria) is involved, along with the chloroplast-encoded PsbN, in the

155 interaction between the D1 and D2 subcomplexes and thus the formation of the RC
156 subcomplex (Komenda et al., 2008; Plücker et al., 2002; Torabi et al., 2014). Further
157 downstream, LPA2 catalyzes a step leading to the formation of stable PSII
158 monomers, probably by facilitating the integration of CP43 into the RC47 subcomplex
159 (Cecchin et al., 2021; Schneider et al., 2014; Spaniol et al., 2021).

160 Chl insertion into nascent D1 is not only required during PSII biogenesis, but also
161 during repair after photoinhibition. Due to accumulation of charge-separated states
162 when photon flux exceeds the capacity for electron transfer, PSII suffers inactivation
163 in high light and even during normal operation of the complex. The D1 protein is the
164 primary target of photodamage, which includes a reversible component, repaired in
165 the absence of protein translation, and an irreversible component that requires
166 degradation of D1 and *de novo* synthesis (for a review see e.g. Theis and Schroda,
167 2016). FtsH is a multi-subunit ATP-dependent thylakoid membrane metalloprotease,
168 combining chaperone and peptidase domains. It has been shown to be a major
169 player in the degradation of D1 and is thus essential for repair after photoinhibition.
170 Land plant mutants of FtsH subunits show variegated leaves (van Wijk, 2015), while
171 in *Chlamydomonas*, *ftsH1* mutants show light-sensitivity and defects in PSII repair
172 (Malnoë et al., 2014). The mutants accumulate damaged D1 and its cleavage
173 products generated by DEG-family endopeptidases. How D1 is extracted from PSII
174 without its total disassembly, and how degradation is coupled with synthesis of a
175 replacement subunit, is still largely unknown.

176 In this study, we show that a null mutant of OHP2 in *Chlamydomonas* is entirely
177 devoid of PSII. The primary defect is a lack of D1 accumulation which can be fully
178 restored by complementation of the mutant with *Arabidopsis* OHP2. Ribosome
179 profiling shows that this defect is not caused by an arrest of *psbA* translation, but by a
180 reduced stability of the newly translated D1 protein. Targeted proteomics show that
181 HCF244 accumulates to ~25% of WT in the *ohp2* mutant, explaining this partial
182 uncoupling between the association of D1 with Chl and the initiation of translation on
183 *psbA*. In the mutant, D1 degradation appears in part mediated by the FtsH protease.
184 An intriguing specificity of *Chlamydomonas* OHP2 is the high-frequency suppression
185 of the PSII-less phenotype in the mutant.

186

187 **RESULTS**

188 **Isolation of a *Chlamydomonas* photosynthetic mutant and identification of the**
189 **mutated locus**

190 By nuclear transformation of the antibiotic resistance marker *aphVIII*, conferring
191 resistance to paromomycin (Pm), we previously generated a collection of insertional
192 mutants of *Chlamydomonas* (Houille-Vernes et al., 2011). The primary screening of
193 this collection combined analysis of fluorescence induction curves with sorting of
194 photosynthetic versus non-photosynthetic (acetate-requiring) phenotypes to
195 categorize the affected photosynthetic complex. The strain *10.1a* was identified as
196 acetate requiring and deficient in PSII. This strain carries a single insertion of the
197 *aphVIII*-cassette in gene *Cre11.g480000* as revealed by inverse PCR and Southern
198 blotting (Supplemental Figure S1A). In a backcross of *10.1a* to the WT strain WT-S34
199 (mt+), the PSII-deficient phenotype segregated 2:2, indicating a single nuclear
200 mutation, but it was neither linked to Pm resistance nor to the cassette inserted in
201 *Cre11.g480000* (Supplemental Figure S1B, top row). This suggested that a second
202 nuclear mutation causes the observed PSII phenotype.

203 Strikingly, all of the 47 PSII-deficient progenies analyzed carried the mating type
204 minus (mt-) gene *MID*, and none the mt+ specific *FUS1* (Supplemental Figure S1B,
205 bottom). This indicates linkage to the mating type locus, a ~1 Mb region of
206 recombinational suppression involved in sex determination, residing on chromosome
207 6 and comprising about 35 genes, many unrelated to sexuality (Ferris et al., 2002).
208 Illumina genome sequencing revealed near the MT locus a single structural variant at
209 position chromosome_6:305949 (v5 genome assembly), i.e. within exon 3 of the
210 *OHP2* gene (*Cre06.g251150*, Figure 1A; Supplemental Figure S2). Analysis of reads
211 flanking this site and their mate reads pointed to the long terminal repeat (LTR)
212 sequence of *TOC1* (Transposon Of Chlamydomonas, Day et al., 1988), indicating a
213 *TOC1* insertion (Supplemental Data S1). Accordingly, Southern blot analysis of the
214 *10.1a* mutant showed integration of a large DNA fragment of ~6 kb into *OHP2* (Figure
215 1B) and none of the 47 PSII-deficient progenies described above gave rise to an
216 *OHP2*-specific PCR-product (Supplemental Figure S1C). To exclude an impact of the
217 initially identified mutation in *Cre11.g480000* on the mutant phenotype, most
218 analyses were performed with a strain of the backcrossed progeny, which we will
219 term *ohp2*, possessing only the mutation in *OHP2* but not the one in *Cre11.g480000*.

220 The *OHP2* gene of *Chlamydomonas* encodes the One-Helix Protein 2 (OHP2)
221 belonging to the Chl *a/b* binding protein superfamily (Engelken et al., 2010). OHP2
222 consists of 144 amino acids with the N-terminal 26 amino acids predicted to
223 represent a chloroplast transit peptide (cTP). The expected mature protein has a
224 molecular mass of 13.4 kDa.

225 **The *ohp2* mutant reveals a complete loss of PSII activity and a reduced Chl** 226 **content**

227 As summarized in Supplemental Table S1, fluorescence induction kinetics and
228 electrochromic shift (ECS) analysis of the *ohp2* mutant revealed a complete lack of
229 PSII, while PSI and *Cytb₆f* activities appeared normal. PSII quantum yield (Fv/Fm)
230 was negative in the *ohp2* mutant because of the small initial drop in fluorescence,
231 typical of mutants completely lacking PSII (Figure 1C, upper panel). This is due to
232 chemical quenching by plastoquinone brought about by the oxidation of plastoquinol
233 by PSI. Similarly, the PSII/PSI ratio, measured from the amplitude of the initial ECS
234 after a flash in the absence and presence of the PSII inhibitors DCMU and
235 hydroxylamine, indicated loss of PSII charge separation (Figure 1C, lower panel).
236 The small effect of the inhibitor treatment on the *ohp2* mutant was ascribed to
237 hydroxylamine and was also observed in PSII-null mutants such as *psbA-FuD7*
238 (Bennoun et al., 1986). Together, these results revealed that PSII activity is
239 completely abolished in the mutant.

240 When cultivated as liquid culture under mixotrophic conditions, the *ohp2* mutant
241 displayed a lighter-green coloration than the wild type (WT) indicative of a slightly
242 lower-level Chl accumulation. Determination of the Chl *a* and *b* content showed that,
243 on a per-cell basis, the *ohp2* strain accumulated only about 58% of the total Chl
244 present in the WT. The Chl *a* content decreased more than the Chl *b* level, leading to
245 a decreased Chl *a*/Chl *b* ratio in *ohp2* (Supplemental Table S1), typical of
246 photosynthetic reaction center mutants.

247 **Complementation of the *ohp2* mutant with *Chlamydomonas* OHP2**

248 Complementation studies were carried out using a plasmid harboring a Pm
249 resistance cassette along with the *OHP2* sequence. We used the full length *OHP2*
250 CDS 3'-terminally fused to a hemagglutinin (HA)-tag encoding sequence, placed

251 under control of the strong nuclear *PSAD* promoter (construct 2 in Supplemental
252 Figure S3). Transformants first selected for Pm resistance were tested for
253 photoautotrophic growth on minimum medium under high or low light. Approximately
254 three quarters of the analyzed clones exhibited restored photoautotrophic growth
255 shown exemplarily for one clone (*ohp2:OHP2-HA* in Figure 1D). This strain was
256 chosen for further experiments, with full restoration of photosynthetic capacities, as
257 judged from its WT-like fluorescence induction and ECS kinetics as well as largely
258 restored Chl accumulation (Figure 1C, Supplemental Table S1). These results
259 confirm that the PSII deficient phenotype of the strain is due to inactivation of *OHP2*.
260 They also show that OHP2 can accommodate a small tag at its C-terminus with no
261 deleterious effect on its functionality.

262 **Functional analysis of the OHP2 protein in *Chlamydomonas***

263 Mature OHP2 from *Chlamydomonas* contains a single C-terminal transmembrane
264 helix including highly conserved residues required for Chl binding (Figure 2A). Based
265 on topology experiments of Li and colleagues (2019) for the *Arabidopsis* OHP2
266 protein (AtOHP2), the less conserved N-terminus of OHP2 should face the
267 chloroplast stroma, while the C-terminus is located on the luminal side. In addition,
268 multiple sequence alignment and hydropathy analysis indicate a well-conserved
269 hydrophobic stretch (HS) of nine residues near the C-terminus which is too short to
270 span the lipid bilayer and seems to be missing in cyanobacterial HLIPs like HliD or
271 HliC (compare Figure 2A; Supplemental Figure S4). This HS might be an
272 evolutionary leftover from a second helix of the ancestral two-helix Stress-Enhanced
273 Proteins (SEP) from which OHP2 potentially originates (Andersson et al., 2003; Beck
274 et al., 2017; Heddad et al., 2012).

275 To test the functional role of this C-terminal hydrophobic region we transformed the
276 mutant with a construct for the expression of a truncated OHP2 protein (pBC1-
277 CrOHP2- Δ HS-HA, construct 5 in Supplemental Figure S3) where the last 14 amino
278 acids are replaced by the HA-tag. Thirty transformants selected on Pm were tested
279 for photoautotrophic growth on minimal medium, but none showed restoration of
280 photoautotrophy (Figure 2B, left panel). No accumulation of the truncated OHP2-HA
281 could be detected in the transformants by immunoblots using an α -HA-antibody
282 (Figure 2B, right panel). These results suggest that even though cyanobacterial

283 orthologs do not have the HS, the last 14 amino acids are essential for OHP2 stability
284 in *Chlamydomonas*.

285 A construct for the expression of a fusion of full-length OHP2 with GFP, adapted to
286 the codon usage of *Chlamydomonas* (CrGFP; construct 3 in Supplemental Figure
287 S3), yielded Pm-resistant transformants, but none was photoautotrophic.
288 Presumably, the large soluble GFP-tag interferes with the function or proper
289 localization of OHP2. However, when we directly fused the predicted transit peptide
290 of OHP2 to CrGFP (construct 4 in Supplemental Figure S3), we observed GFP
291 protein accumulation in two out of eight immunologically analyzed clones upon
292 transformation of the *UVM4* strain which is known for its high capacity to express
293 nuclear transgenes (Supplemental Figure S5A, upper panel; Neupert et al., 2009).
294 Confocal laser scanning microscopy of one transformant showed that the GFP
295 fluorescence signal co-localized with the Chl autofluorescence in the single cup-
296 shaped chloroplast (Supplemental Figure S5A, lower panel), clearly distinct from the
297 cytosolic control (CrGFP). Moreover, immunological analysis of cellular subfractions
298 of the strain *ohp2:OHP2-HA* described above revealed a membrane localization of
299 the ~14 kDa OHP2-HA tagged protein comparable to that of the integral thylakoid
300 membrane protein D2 (Supplemental Figure S5B).

301 Taken together, these results indicate that OHP2 is a thylakoid membrane-
302 localized protein. Moreover, while a C-terminal fusion of a small tag to OHP2 still
303 allows the protein to fulfil its native function, removal of its C-terminus or introduction
304 of a large GFP tag severely impairs its function and /or stability.

305 **Reduced PSII subunit accumulation and synthesis in the *ohp2* mutant**

306 As judged from the analysis of photosynthetic parameters in the *ohp2* mutant, in
307 particular the lack of effect on PSI, OHP2 appears exclusively involved in PSII
308 biogenesis. Accordingly, immunoblot analyses revealed no change in the
309 accumulation of the large subunit of Rubisco (RbcL), the PSI reaction center protein
310 PsaA or Cyt f of the Cyt b_6/f complex (Figure 3A). In contrast, the PSII core proteins D1
311 and D2 were below the detection limit. Typical for mutants lacking D1 or D2, the core
312 antenna protein CP43 accumulated to some extent, about 12% of the level in WT
313 (Figure 3A). Complementation of *ohp2* with the *OHP2* cDNA fully restored protein
314 accumulation in the strain *ohp2:OHP2-HA* (Figure 3A).

315 To exclude that the *OHP2* mutation affects the accumulation of *psbA* and *psbD*
316 transcripts, encoding D1 and D2 proteins, respectively, total RNAs were subjected to
317 Northern blot analysis. However, no significant alteration of *psbA* and *psbD* transcript
318 accumulation was observed in *ohp2* when compared to the WT (Figure 3B). To
319 determine whether the mutation instead affects translation or prevents stabilization of
320 chloroplast-encoded PSII subunits, ¹⁴C pulse chase labeling experiments were
321 carried out in the presence of cycloheximide (Figure 3C). Both independently grown
322 *ohp2* cultures revealed a reduction of radiolabeled CP47, and to a lower extent of
323 CP43 and D2 proteins in comparison to the WT. However, the most significant effect
324 was observed for the D1 protein for which no incorporation of the radiolabel was
325 detected, neither during the pulse nor after the chase. This suggests that the primary
326 defect in the *ohp2* mutant is either a deficiency in D1 synthesis or a very fast
327 degradation of newly synthesized D1 proteins. The effects on other PSII subunits
328 may be ascribed to assembly-dependent translational control (CES; Choquet and
329 Wollman, 2009) or reduced stability of the unassembled subunits.

330 Our efforts to raise a functional antibody against recombinant OHP2 having
331 failed, we used the *ohp2:OHP2-HA* strain, along with the WT and *ohp2*, to examine
332 the assembly of PSII and the location of OHP2. Crude membrane fractions were
333 solubilized and subjected to 2D-BN/SDS-PAGE (Figure 3D). As anticipated from the
334 unaffected accumulation of the PSI subunit PsaA (Figure 3A), all PSI-related
335 complexes, including PSI core and supercomplexes, were assembled in the *ohp2*
336 mutant. Remarkably, a higher ratio of PSI supercomplexes to PSI core complexes
337 was observed in the *ohp2* mutant, suggesting that LHCl antenna in this strain is more
338 tightly coupled to the PSI core than in the WT. This phenomenon was only partially
339 reverted in the complemented strain. All PSII complexes formed in the WT were
340 below the detection limit in the absence of the OHP2 protein. In agreement with the
341 restored photoautotrophic growth and PSII protein accumulation in the
342 complemented strains, all PSII related complexes were present in the analyzed
343 *ohp2:OHP2-HA* strain. Interestingly, different from *Arabidopsis*, where AtOHP2 was
344 detected as a distinct signal at the size of a ~150 kDa PSII RC-like complex (Li et al.,
345 2019), the HA-tagged OHP2 protein in our complemented strain was mainly detected
346 in the low molecular range, reaching up as a weak smear to the first monomeric
347 CP43-less PSII RC47 subcomplex (Figure 3D). This suggests that in

348 *Chlamydomonas* the putative OHC, if existing, is smaller in size or does not
349 withstand the conditions used for BN-PAGE.

350 **Ribosome profiling reveals that D1 is still translated in the absence of OHP2**

351 Based on the molecular characterization of the *ohp2* mutant, the major effect of the
352 loss of OHP2 in *Chlamydomonas* seems to be the missing accumulation of the PSII
353 reaction center protein D1, in line with observations in other organisms. However, our
354 ¹⁴C pulse labelling experiments (Figure 3C) can be interpreted either as an absence
355 of translation of the *psbA* mRNA or as a very rapid or even co-translational
356 degradation of newly synthesized D1. To address this question and obtain a
357 quantitative image of chloroplast translation in the *ohp2* mutant, we employed a
358 previously established targeted chloroplast ribosome profiling approach, which is
359 well-suited to dissect mutant defects of translation (Trösch et al., 2018). Ribosome
360 footprints (FP) from WT and mutant were extracted and analyzed by hybridization of
361 highly tiled microarrays covering all open reading frames of the chloroplast genome.
362 In parallel, total RNA was isolated, fragmented and detected by the same approach.
363 Direct correlation between the three biological replicates showed a high
364 reproducibility both for determining RNA accumulation ($r > 0.96$) and translation
365 output ($r > 0.93$) (Supplemental Figure S6A, Supplemental Dataset 1).

366 General gene expression defects were examined by averaging all probe intensities
367 for mRNA or ribosome FPs that covered individual chloroplast CDSs, respectively.
368 Direct plotting of mRNA intensities showed highly comparable RNA abundances
369 between the WT and the mutant ($r = 0.98$, Figure 4A). This suggests that the lack of
370 OHP2 is not causing any obvious transcription or RNA stabilization defects. In
371 contrast, the translational output, as determined by relative FP abundance for each
372 ORF, revealed clear differences between mutant and WT cells and hence, reduced
373 correlation ($r = 0.9$, Figure 4A).

374 Unexpectedly, averaged FP intensities of *psbA* showed only a mild reduction in the
375 mutant (Supplemental Dataset 1). FP abundance was reduced by less than 2-fold,
376 which combined with a slight reduction in mRNA abundance, led to a practically
377 unchanged translation efficiency (Figure 4B). For a more detailed view, we also
378 plotted ribosome occupancy (\log_2 of the *ohp2*/WT ratio) over the *psbA* ORF (Figure
379 4C, left panel). A more pronounced reduction (up to 4-fold) in ribosome occupancy in
380 *ohp2* can be observed over the first half of the ORF (~160 codons, up to the 3rd

381 transmembrane segment of nascent D1). In the second half, only mild reduction or
382 even a slight increase in ribosome occupancy could be detected. For other PSII
383 subunits, the most pronounced was the reduced translation of CP47 (PsbB), PsbH,
384 and PsbT, with up to 3-fold lower translation output for *psbB* (Figure 4B and
385 Supplemental Figure S6B). This observation agrees with the hierarchical CES
386 cascade contributing to the biogenesis of PSII in *Chlamydomonas*, where the
387 presence of D2 is required for high-level translation of D1, which in turn is a
388 prerequisite for efficient translation of the core antenna protein CP47 (Figure 4D;
389 reviewed in Choquet and Wollman, 2009). When assembly of D1 and CP47 subunits
390 is compromised, the unassembled proteins repress the translation initiation of their
391 encoding mRNA (Minai et al., 2006). Also, in accordance with previous investigations
392 of PSII mutants (de Vitry et al., 1989), we observed no effect on translation of the
393 second inner antenna protein CP43, encoded by the *psbC* mRNA, confirming that its
394 rate of synthesis is not dependent on the assembly with other PSII subunits.

395 Interestingly, also PsbH, which only recently has been hypothesized to be part of
396 the CES cascade downstream of D1 (Trösch et al., 2018), exhibited a clearly reduced
397 translation output in *ohp2*, thus further supporting its role as a CES subunit (Figures
398 4A, 4B, 4D). A comparable effect was seen for the translation of *psbT*. Remarkably,
399 the three affected genes are encoded in the *psbB-T-H* operon. To obtain a more
400 detailed view on the translation of this polycistronic transcript, we further looked at
401 relative ribosome FP accumulation along this *psbB-T-H* operon, calculated as mean
402 \log_2 ratios to directly compare mRNA abundance and ribosome occupancy between
403 mutant and WT. While the RNA of the operon was only marginally reduced, a clear
404 and relatively even reduction of ribosome occupancy was seen for all ORFs (Figure
405 4C, right panel). It is noteworthy that also *psbN*, which is positioned between *psbT*
406 and *psbH* in antisense orientation, exhibits a reduced translational efficiency while
407 the mRNA levels appeared slightly increased. PsbN acts as an assembly factor for
408 PSII but is not part of the final complex.

409 Complementary dynamics were observed for the synthesis of D2, which showed
410 increased ribosome FP intensities over the entire ORF in *ohp2* while maintaining
411 constant mRNA abundance (Figures 4A, 4B, Supplemental Figure S7). As D2 is the
412 dominant CES subunit (Figure 4D), this likely points to a compensatory effect caused
413 by the lack of functional PSII. Similarly, other translational alterations in *ohp2*, like the
414 reduction of ribosome FPs for the large Rubisco subunit RbcL or an upregulation of

415 all chloroplast-encoded ATP synthase subunits (Supplemental Figure S6), may rather
416 be secondary effects caused by a diminished photosynthetic electron flow and/or
417 energy limitation.

418 **Proteomic analysis reveals the presence of HCF244 in the *ohp2* mutant**

419 For a quantitative and comprehensive view on the proteome composition in the *ohp2*
420 mutant, proteomic shot-gun analysis was conducted on whole cell fractions (Figure
421 5A, Supplemental Dataset 2). The analysis additionally included an *ohp2* strain in
422 which the PSII phenotype was suppressed. Such photoautotrophic suppressor
423 strains occurred at a high frequency (approximate rate: 5.5×10^{-6}) under conditions
424 selecting for photoautotrophic growth. Illumina sequencing and Southern blot
425 analysis of photoautotrophic *ohp2* derivatives showed that they still contained the
426 *TOC1* transposon in *OHP2* (Supplemental Figures S2, S8A), indicating suppression
427 of the PSII phenotype by a second site mutation. The suppressor strains showed
428 partially restored photosynthetic parameters (Fv/Fm ratios of 0.46-0.64), a re-
429 accumulation of PSII subunits indicated by restored D2 levels, and the ability to grow
430 photoautotrophically in liquid medium under strong illumination (Supplemental
431 Figures S8B-D). We proteomically analyzed suppressor strain *M-Su1* to distinguish
432 the direct effects of the lack of OHP2 from those linked to PSII loss. In addition, LC-
433 MS analysis was carried out on membrane fractions of WT, *ohp2* and the suppressed
434 strain (Figure 5B, Supplemental Dataset 3). These two analyses allowed reliable
435 quantification of 3065 and 1127 proteins, respectively, with very high reproducibility
436 between the biological replicates (Supplemental Figure S9A). The complemented
437 strain *ohp2:OHP2-HA* was included as a control, and showed that most of the
438 alterations observed in mutant cells were reverted by complementation
439 (Supplemental Figure S9B). The most obvious defect observed in the *ohp2* strain,
440 apart from the expected absence of OHP2 itself, was a severe depletion of the
441 majority of PSII proteins. The most dramatic effect was on D1 showing a ~200/640-
442 fold reduction in whole cell and membrane fractions, respectively. Notably, the
443 detection in the *ohp2* mutant of five D1 peptides arising from the C-terminal third of
444 the protein supports the notion, based on the results of the ribosome footprinting, that
445 the *psbA* CDS is translated over its entire length. For the other large PSII subunits D2
446 and CP47, the depletion was less pronounced. The least affected subunit was CP43,
447 in accordance with results obtained with other PSII mutants (de Vitry et al., 1989).

448 The small molecular weight subunits of PSII were difficult to assess in these
449 experiments, but we noticed a massive depletion of PsbH in the mutant
450 (Supplemental Datasets 2, 3), in agreement with the ribosome profiling results. Other
451 PSII subunits were severely depleted, at least at the membrane level, including the
452 newly-discovered algae-specific subunit PBAS1 (= PBA1, Putatively Photosystem B
453 Associated 1; Spaniol et al., 2021). Among the extrinsic luminal Oxygen-Evolution
454 Enhancer (OEE) subunits, no significant change was observed in whole cells, but
455 OEE1 was depleted in membranes, in line with previous reports (de Vitry et al.,
456 1989).

457 Of particular interest for us was the presence in the mutant and suppressor strains
458 of OHP1 and HCF244, partners of OHP2 in the OHC. Probably due to its small size
459 and hydrophobicity, OHP1 was detected neither in the whole cell extracts nor in the
460 untargeted analysis of membrane fractions, even in the WT. To further refine our
461 analysis, the same membrane fractions were also subjected to a targeted proteomics
462 approach, whereby specific peptides were monitored at high resolution. By reducing
463 interferences from the MS1 level, this allows a more reliable quantitation. Five
464 proteins were selected: OHP2, OHP1, HCF244, HCF136 and HCF173, using a total
465 of 25 peptides (Figure 5C and Supplemental Dataset 4). This targeted analysis used
466 two peptides for OHP1 and showed a low signal in membrane fractions of the *ohp2*
467 mutant (18% of WT). This suggests that in *Chlamydomonas*, OHP1 is not completely
468 dependent on OHP2 for its stabilization. The OHP1 signal was not detected in the
469 suppressed strain.

470 In whole cell extracts, HCF244 accumulated to ~25% of the WT level in *ohp2* and
471 in the suppressor strain (Supplemental Dataset 2). Like OHP2 accumulation, this was
472 largely complemented by expression of the *OHP2-HA* transgene. Untargeted
473 analysis of the membrane fractions revealed the presence of HCF244 in the WT but
474 not in *ohp2* or the suppressed strain. However, the more sensitive targeted analysis,
475 based on eight peptides, revealed the presence of HCF244 in the membrane
476 fractions of the mutant and suppressor strains, with an abundance of 22% and 13%
477 relative to WT levels, respectively (Supplemental Dataset 4, Figure 5C). Together,
478 these results indicate, that in contrast to *Arabidopsis*, the presence of OHP2 is not
479 absolutely necessary for HCF244 accumulation, nor for its association with the
480 membrane.

481 **Proteomic analysis of other PS subunits, assembly factors and chloroplast**
482 **enzymes**

483 We also examined the accumulation of other known PSII biogenesis factors, in
484 search of secondary effects of the lack of OHP2, or possible mechanisms or
485 consequences of suppression (Figure 5; Supplemental Datasets 2 - 4). At the whole
486 cell level, the abundance of HCF173 was not affected in the mutant or suppressor,
487 but targeted analysis of the membrane fractions revealed a ~3-fold higher level in
488 *ohp2*, compared to the WT or suppressed strains, suggesting a regulatory
489 mechanism. Another known interactant of the *psbA* mRNA in plants is SRRP1: its
490 abundance was significantly increased in the *ohp2* mutant cells and restored to
491 normal by complementation. In the suppressor strain, SRRP1 was barely detectable.
492 Similarly, the *psbA* translation activator TBA1 (Somanchi et al., 2005)
493 overaccumulated in the mutant.

494 The luminal protein HCF136 is an early interactant of the D2/Cytb₅₅₉ pre-complex,
495 necessary for assembly of pD1 into the RC (Plücken et al., 2002). Its abundance in
496 whole cells was not significantly altered, but both the untargeted and targeted
497 analyses of the membrane fractions revealed a significantly higher membrane
498 association in the suppressor strain (~3-fold when compared to the WT; Figure 5;
499 Supplemental Datasets 2 - 4). This may reveal a more prolonged association of
500 HCF136 with the RC when the absence of OHP2 slows down the biogenesis
501 process.

502 PSB28 binds to CP47 on the stromal surface and distorts the Q_B-binding pocket,
503 as revealed by the structural analysis of a cyanobacterial PSII assembly intermediate
504 also comprising PSB27, which binds to CP43 and the transmembrane protein PSB34
505 on the luminal side (Xiao et al., 2021; Zabret et al., 2021). Here, PSB28 and PSB27
506 showed interesting contrasted behaviors. At the whole cell level, the accumulation of
507 PSB28 showed no significant change between strains. However, it was undetectable
508 in the membrane of the *ohp2* strain and of the suppressor. In contrast, PSB27 was
509 overaccumulated in *ohp2* cells, with no change in its abundance in membrane
510 fractions. The suppressor also showed some overaccumulation of PSB27, this time
511 accompanied by a marked increase in its association with the membrane. In the
512 mutant, we also noticed an increased accumulation of PSB33/TEF5, a factor involved
513 in the interaction of photosystems and antenna complexes (Fristedt et al., 2015;
514 Nilsson et al., 2020) and of APE1, which has been described as involved in the

515 adaptation to high light (Walters et al., 2003) and found as a specific interactant of
516 *Arabidopsis* OHP1 in pull-down assays (Myouga et al., 2018). Finally, we observed
517 increased membrane association of PSB29/THF1 in the mutant, which was partially
518 reverted in the suppressor strain. THF1 has been shown to be involved in the
519 dynamics of PSII-LHCII supramolecular organization and to associate with the FtsH
520 protease (Bečková et al., 2017; Huang et al., 2013; Wang et al., 2004).

521 In contrast to PSII, no significant effect was observed on the accumulation of PSI
522 RC subunits: the slight overaccumulation of PSAE in whole cells of the mutant was
523 also found in the suppressed and complemented strains and may therefore be
524 unlinked to OHP2. More interestingly, however, all the LHCI subunits showed
525 increased accumulation in the *ohp2* mutant as well as in the suppressor strain,
526 suggesting a direct effect of the lack of OHP2 (Supplemental Dataset 2). While
527 subunits of the *Cytb₆f* complex appeared unaffected in the *ohp2* mutant, we noticed
528 an overaccumulation of those of the ATP synthase (Figure 5A, left panel). This
529 agrees with the increased translational output for the ATP synthase ORFs seen in our
530 ribosome profiling analysis (Supplemental Figure S6B). Overaccumulation of the ATP
531 synthase was fully reversed in the complemented strain (Supplemental Figure S9B).
532 We note, however, that the suppressor strain, although photoautotrophic, still showed
533 some overaccumulation of the ATP synthase in its membrane fraction (Figure 5B).
534 The Rubisco subunits RbcL and RBCS2, in contrast, appeared to accumulate at
535 lower levels in the mutant in whole cells fractions (Supplemental Dataset 2). The
536 significance of this observation is unclear, as their accumulation was not restored to
537 normal in the suppressor strain.

538 Several enzymes of the porphyrin biosynthesis pathway showed changes in their
539 accumulation or association with the membrane (Supplemental Datasets 2, 3,
540 Figures 5A, 5B). The Chl synthase CHLG, whose cyanobacterial homolog interacts
541 with HliD/Ycf39 (Chidgey et al., 2014), remained unaltered in the *Chlamydomonas*
542 mutant, but other Chl synthesis enzymes showed increased abundance in the
543 membrane fractions. This includes the two subunits of the Mg-chelatase (ChIH, ChII),
544 the Mg protoporphyrin IX S-adenosyl methionine O-methyl transferase ChIM, the
545 cyclases CRD1 and CTH1 and the protochlorophyllide *a* oxidoreductase POR1.
546 Except for POR1, this increase was not observed at the whole cell level, suggesting
547 that the cell responds to the absence of the OHC complex by stabilizing the
548 interaction between these Chl pathway enzymes and the thylakoid membrane. This

549 effect was largely or completely reversed in the suppressor, pointing to a regulatory
550 mechanism compensating for the impaired stabilization of D1. In the upstream part of
551 the pathway, shared with heme biosynthesis, several enzymes overaccumulated in
552 whole cells of the mutant (Figure 5A): the delta-aminolaevulinic acid dehydratase
553 (ALAD1), the uroporphyrinogen III synthase (UPS1), one of the three
554 uroporphyrinogen III decarboxylases (UPD1), and the protoporphyrinogen oxidase
555 (PPX1). PPX1 abundance also increased in the membrane fraction. The protein
556 FLUORESCENT (FLU), which is involved in the regulation of the whole pathway
557 (Falciatore et al., 2005) and which was severely reduced in a virus-induced *OHP2*
558 gene silenced *Arabidopsis* line (Hey and Grimm, 2018), was not significantly affected
559 in the *Chlamydomonas* mutants.

560 **The *Arabidopsis* OHP2 complements the *Chlamydomonas ohp2* mutation**

561 The observed phenotypical differences between *ohp2* mutants from higher plants and
562 *Chlamydomonas*, as well as the divergence of the amino acid sequences (Li et al.,
563 2019; Myouga et al., 2018) led us to test whether the *Arabidopsis* protein could
564 complement the *Chlamydomonas* mutant. The N-terminal region of the mature OHP2
565 proteins is much less conserved than the transmembrane and C-terminal regions and
566 similarity between the *Chlamydomonas* and *Arabidopsis* proteins starts only at
567 residue 65 of the *Chlamydomonas* OHP2 preprotein with an overall identity of 58%
568 (compare Figure 2A).

569 We used a construct (pBC1-TP_{CrOHP2}-AtOHP2-HA, construct 6 in Supplemental
570 Figure S3) fusing the predicted cTP of OHP2 from *Chlamydomonas* with a codon-
571 adapted sequence encoding the mature part of AtOHP2 (Supplemental Data S2).
572 After transformation of the *Chlamydomonas ohp2* mutant and selection for Pm-
573 resistance, 17 of the 20 clones (85%) showed restoration of photoautotrophy and
574 Fv/Fm values of 0.62 – 0.74 (Supplemental Figure S10A). For all of the
575 immunologically analyzed clones, a protein with the expected size of ~ 15 kDa was
576 detected using the α -HA-tag antibody and D1 proteins accumulated to WT levels
577 (Supplemental Figure S10B). Taken together these data indicate WT level PSII
578 accumulation and successful complementation of the *Chlamydomonas* mutant with
579 the *Arabidopsis* protein.

580 **Slowing down D1 degradation in the *ohp2* mutant can partially restore light-**
581 **sensitive PSII activity, but not photoautotrophy**

582 The repair of photodamaged PSII involves the selective proteolytic degradation and
583 replacement of the damaged D1 polypeptide with a newly synthesized one (reviewed
584 in Kato and Sakamoto, 2009; Nixon et al., 2010). The thylakoid protease FtsH plays a
585 major role in the D1 degradation process. In *Chlamydomonas*, FtsH is composed of
586 two subunits FtsH1 and FtsH2 and the *ftsH1-1* mutation, changing a conserved
587 arginine residue, strongly impairs oligomerization and proteolytic activity (Malnoë et
588 al., 2014). This mutation restores photosynthesis in a mutant lacking heme c_i of
589 *Cytb₆f* (Malnoë et al., 2011). In addition, it impairs degradation of D1 in high light,
590 slowing down repair of PSII during photoinhibition and leading to enhanced light-
591 sensitivity in mixotrophic and photoautotrophic conditions (Malnoë et al., 2014). To
592 address the question whether the FtsH protease is involved in the immediate post-
593 translational degradation of D1 in the *ohp2* mutant, we crossed the original *10.1a*
594 strain with a strain carrying the *ftsH1-1* mutation. In the progeny, the phenotypes
595 associated with the WT, *ohp2*, *ohp2 ftsH1-1* and *ftsH-1* genotypes showed distinct
596 fluorescence and growth patterns (Figure 6). When strains were analyzed by spot
597 tests on agar plates, the *ftsH1-1* strains showed retarded growth and decreased
598 Fv/Fm with increasing light intensity under photoautotrophic as well as under
599 mixotrophic conditions (Figure 6A). This is typical of the *ftsH1-1* light-sensitive
600 phenotype (Malnoë et al., 2014). As expected, the *ohp2* progeny did not grow
601 photoautotrophically, except for occasional suppressor clones. Under mixotrophic
602 conditions, they showed no deleterious effect of high light for growth, as is typical of
603 PSII mutants, and had practically no Fv/Fm (Figures 6A, 6B). The *ohp2 ftsH1-1*
604 strains showed interesting phenotypes. Like the *ohp2* parent, they were unable to
605 grow on minimal medium at any light intensity tested (Figure 6A). However, their
606 fluorescence induction curves were clearly indicative of the presence of a small
607 amount of PSII, especially in dark-grown cells (Figure 6C). On TAP, we did not
608 observe any stimulatory effect of low light on growth (Figure 6A). These results
609 suggest that FtsH is involved in the degradation of the PSII units, possibly abnormal,
610 produced in *ohp2* mutants. However, the activity of the low amount of PSII stabilized
611 by attenuation of FtsH is either insufficient or too light-sensitive to allow
612 photoautotrophy. Note that the unknown suppressor locus was not genetically linked

613 to *FTSH1* in crosses, and the suppressor strains showed no sequence change in any
614 of the *FTSH* genes, nor in any other known chloroplast protease gene.
615

616 DISCUSSION

617 In *Chlamydomonas*, OHP2 is not necessary for *psbA* translation.

618 The molecular analysis of an *ohp2* knockout mutant from *Chlamydomonas* revealed
619 a major defect in PSII biogenesis, as indicated by its inability to grow
620 photoautotrophically, the complete loss of PSII activity and the absence of the major
621 PSII subunits, in particular D1 (Figures 1, 3). No effect was observed on the PSI RC
622 (Figures 1C, 3A, 3D, 5), as reported for cyanobacteria (Komenda and Sobotka,
623 2016), but at slight variance with land plants, where reductions in PSI subunits and
624 antenna proteins have been reported (Beck et al., 2017; Li et al., 2019; Myouga et
625 al., 2018). In *Chlamydomonas*, we unexpectedly observed an increased
626 accumulation of LHCl antenna proteins in the mutant (Supplemental Dataset 2), and
627 a higher abundance or stability of the PSI-LHCl complex in non-denaturing PAGE
628 (Figure 3D). Whether this is related to the observed decrease in Chl abundance and
629 changes in expression of Chl pathway genes remains to be investigated.

630 In other organisms, a dimer of One-Helix Proteins (HliC/D in cyanobacteria,
631 OHP1/2 in land plants) has been found to mediate the early association of Chl *a* to
632 the nascent D1 polypeptide. In *Chlamydomonas*, the expression patterns of OHP2,
633 OHP1 and HCF244 in a variety of conditions are highly similar (Supplemental Figure
634 S11) and on the Phytozome website (<https://phytozome-next.jgi.doe.gov/>) the latter
635 two appear in each other's lists of best correlated genes, pointing to the existence of
636 a similar complex in the alga. In the *Chlamydomonas ohp2* mutant, we will therefore
637 assume that the absence of such an OHC causes the lack of cofactor insertion into
638 D1, resulting in the loss of protein accumulation. Note that, although Chl is usually
639 mentioned as the essential cofactor missing in *ohp2*, Phe *a* is also a likely substrate
640 for the action of the OHC. The main result of our study, compared with those in
641 higher plants, is that in *Chlamydomonas* the absence of OHP2 does not lead to the
642 inability to translate the *psbA* mRNA. While our ¹⁴C pulse labelling experiments do
643 point to the primary phenotype being a defect in D1 production, they can be
644 interpreted either as a deficiency in *psbA* translation, or as a very fast degradation of
645 the newly synthesized D1 polypeptide (Figure 3C). Our ribosome profiling
646 experiments strongly support the latter hypothesis, as they show an almost normal
647 abundance of FPs over the CDS, indicating continued translation of the *psbA* mRNA
648 over its whole length (Figure 4C). This is further supported by the fact that the

649 proteomic analysis identified several peptides in *ohp2* that lie in the C-terminal part of
650 D1.

651 Note that the two techniques we have used have their limitations. Usually, the
652 absence of a signal in ^{14}C -pulse labeling in *Chlamydomonas* is interpreted as loss of
653 translation (e.g. de Vitry et al., 1989). But the *ohp2* mutant must be analyzed
654 differently, as the mutation is supposed to affect a co-translational or early post-
655 translational step. In addition, the sensitivity of this approach is limited by the
656 broadness of the D1 band (D originally stands for "diffuse") and the unavoidable
657 presence of background radioactivity. Ribosome footprinting is more sensitive, even
658 though it also is an indirect proxy for translation initiation. The abundance of RFs over
659 a transcript may also be affected by the dynamics of translation, for example the
660 stalling of ribosomes will increase the probability to generate RFs at this position. It is
661 interesting to note that the reduction in ribosome occupancy in the *ohp2* mutant is
662 more pronounced over the first half of the mRNA. Chl attachment to D1 has been
663 proposed in barley to be associated with ribosome pausing (Kim et al., 1994a; Kim et
664 al., 1991, 1994b) even though RF experiments in maize have failed to identify such
665 Chl supply dependent pauses (Zoschke and Barkan, 2015; Zoschke et al., 2017). If
666 interaction of the nascent chain with the Chl attachment machinery slows down
667 elongation, then its absence in *ohp2* may reduce the density of RFs. Conservatively,
668 we propose that in the absence of OHP2, *psbA* translation is maintained at a
669 significant rate, over the whole CDS. However, the degradation of apo-D1 is so fast
670 that full-length D1 remains below detection in pulse labeling experiments, as it is in
671 Western blots (Figures 3A, 3C). This statement is backed by the observation that
672 mutations in the FtsH protease and at an unknown suppressor locus can partially or
673 fully restore PSII accumulation, which would be difficult to achieve if OHP2 was
674 required for translation.

675 The situation is different in land plants, where OHP1, OHP2 and HCF244 are
676 required for the recruitment of ribosomes to the *psbA* mRNA (Chotewutmontri et al.,
677 2020). The abundance of RFs in the *Arabidopsis ohp2-1* knockout mutant was ~12
678 times lower than in the WT, and probably overestimated by normalization since the
679 *psbA* CDS itself contributes to a large fraction of the RFs in the WT. Chotewutmontri
680 et al. convincingly explained the discrepancy with a previous study using polysome
681 analysis (Li et al., 2019), by the difficulty in analyzing *psbA* polysomes profiles due to
682 the high abundance of the mRNA. They found that the *Arabidopsis ohp1-1* and maize

683 *hcf244-1/-3* null mutants also fail to translate D1 (6-fold and 10-fold reduction,
684 respectively). No change was observed in the pattern of RFs over *psbA* in any of the
685 mutants, in line with a defect in translation initiation rather than elongation. All this
686 was in accordance with the role of HCF244 as an essential translation initiation factor
687 for *psbA* and its total absence in mutants lacking OHP1 or OHP2 (Li et al., 2019).
688 Chotewutmontri and coworkers recently proposed a model for regulation of *psbA*
689 translation by light, whereby the D1-bound OHC inhibits the ability of the stroma-
690 exposed components (HCF244 and/or OHP2's stromal tail) to initiate *psbA*
691 translation (Chotewutmontri and Barkan, 2018; 2020; Chotewutmontri et al., 2020). It
692 must be noted that Chotewutmontri et al. (2020) quantified RFs by Illumina read
693 counting, while we have used hybridization to oligonucleotide probes. But both
694 methods are fully validated, and the results are so different that we cannot invoke a
695 technical bias. Therefore, we conclude that *Chlamydomonas* lacks the OHP2-
696 dependent control mechanism for *psbA* translation described in land plants.

697 We used proteomics analyses to explain this apparent discrepancy in the context
698 of the high conservation of the proteins between algae and land plants (as
699 exemplified by our observation that *Arabidopsis* OHP2 can complement the
700 *Chlamydomonas* mutant; Supplemental Figure S10). Quantification of OHP1 was
701 difficult because of its small size, but the results of our targeted analysis point to the
702 presence of traces of this protein in the *ohp2* mutant (Figure 5C). This, however,
703 should have no effect on the insertion of cofactors: an *ohp2* mutation in *Arabidopsis*
704 is not complemented by overexpression of OHP1 (Beck et al., 2017) and OHP1 alone
705 does not bind pigments *in vitro* (Hey and Grimm, 2020). Studies in land plants have
706 found that while some OHP2 can accumulate in *ohp1* null mutants, OHP1 is usually
707 undetectable in *ohp2* mutants (Beck et al., 2017; Li et al., 2019). Some variability is
708 seen in these studies, possibly due to the fact that the T-DNA insertion in *OHP2* lies
709 within an intron (Beck et al., 2017; Li et al., 2019; Myouga et al., 2018). Similarly, the
710 level of HCF244 reported in *Arabidopsis ohp2* mutants varied from nil to very low (Li
711 et al., 2019) and the accumulation of HCF244, even when overexpressed, was found
712 to be limited by that of OHP2 (Hey and Grimm, 2020; Li et al., 2019). Here, our
713 untargeted and targeted LC-MS/MS analyses concur to demonstrate not only that
714 HCF244 accumulates to significant levels in the *Chlamydomonas ohp2* mutant
715 (~25% of WT), but that it can interact with the membrane (Figure 5C). This might be
716 explained by the remaining traces of OHP1 acting as an anchor for HCF244 and

717 stabilizing it, or to an intrinsically higher stability of *Chlamydomonas* HCF244 when
718 not assembled. We propose that these remaining 25% HCF244 in the
719 *Chlamydomonas ohp2* mutant are responsible for the maintenance of *psbA*
720 translation at an appreciable rate. This does not exclude that an autoregulatory circuit
721 exists in WT *Chlamydomonas* similar to that described by Chotewutmontri and
722 Barkan (2020) in land plants. In this case, the absence of OHP1/OHP2 in the mutant
723 may prevent the remaining HCF244 from sensing the presence of unassembled D1,
724 leading to enhanced activation of *psbA* translation. In any event, the strong coupling
725 observed in plants between Chl insertion and *psbA* translation initiation appears
726 largely broken in *Chlamydomonas*. This coupling may be ancient in oxygenic
727 photosynthesis, as judged from the existence of a similar complex in cyanobacteria. It
728 might be interesting to examine whether the cyanobacterial complex also controls
729 *psbA* translation. A major difference between *Arabidopsis* and *Chlamydomonas* is
730 that Chl production depends entirely on light in the former, while the latter can
731 produce it in the dark. Thus, the availability of Chl for integration into PSII could be
732 used by Angiosperms to sense light, while algae (and cyanobacteria) would have to
733 use other clues. In addition, the translation of *psbA* appears to mobilize a larger
734 fraction of ribosomes in the plant than in the alga, as judged from RF and pulse-
735 labeling experiments. Arguably, the alga can partly dispense of a regulatory circuit
736 aimed at ensuring that *psbA* is translated only in the light. Detailed studies in other
737 systems, such as land plants capable of producing Chl in the dark, are necessary to
738 decide how strong the coupling needs to be to prevent deleterious effects of
739 uncoordinated D1 synthesis and assembly, in particular during high light stress when
740 D1 needs to be repaired at high rate.

741 **The absence of OHP2 affects translation of several chloroplast transcripts**
742 **encoding PSII subunits**

743 Interestingly, the *ohp2* mutant revealed large changes in the ribosome profiling
744 pattern of PSII transcripts other than *psbA*. Most striking was the reduced
745 translational output for the CES subunit CP47, encoded by *psbB* (Figure 4). This
746 observation is in line with previous knowledge on translational regulation by assembly
747 (the CES process) in *Chlamydomonas* (reviewed in Choquet and Wollman, 2009;
748 Minai et al., 2006). Genetic studies indeed have demonstrated that in the absence of
749 D1, the unassembled CP47 subunit feeds back onto the translation initiation of its

750 own mRNA. Here, assuming that no assembly of CP47 and D1 can occur in the *ohp2*
751 mutant, we can quantify this effect. With a 3-fold reduction of RFs over the *psbB*
752 mRNA in the mutant ($\log_2 \text{ohp2/WT} = -1.58$), the CES effect appears to be rather
753 dramatic (Figure 4B). Remarkably, the translation of *psbH* is also reduced in the
754 mutant, in line with a complete lack of detection of PsbH peptides by proteomic
755 analyses (Supplemental Datasets 2, 3). This supports the identification of PsbH as a
756 component of the PSII CES cascade, as proposed recently by Trösch et al. (2018;
757 Figure 4D). Early reports in *Chlamydomonas* describe a role of PsbH in assembly
758 and/or stabilization of PSII (O'Connor et al., 1998; Summer et al., 1997) but the
759 protein's function has not been studied in detail. In the cyanobacterium
760 *Synechocystis sp.* PCC 6803, PsbH is associated with CP47 and facilitates D1
761 processing and incorporation into PSII (Komenda et al., 2005). Assuming a similar
762 position of PsbH in the assembly pathway in *Chlamydomonas*, its CES-mediated
763 downregulation in the absence of D1 is consistent with that of CP47. The mechanism
764 remains to be determined: is this regulation dependent upon the accumulation of
765 unassembled PsbH, unassembled CP47 or the CP47/PsbH sub-complex? Genetic
766 studies using mutants lacking the CP47 or PsbH proteins will be necessary to
767 address this question. In their study, Chotewutmontri et al. (2020) pointed to an
768 increased, rather than decreased, translation of *psbB* in their *ohp1*, *ohp2*, *hcf244* and
769 even in *hcf173* mutants. The significance of these opposite behaviors between
770 *Chlamydomonas* and land plants remains to be explored. Noticeably, *psbH*,
771 compared to other PSII subunits, also appeared as slightly increased in the RF
772 abundancy plots of the *ohp2* and *hcf244* mutants in Chotewutmontri et al. (2020).

773 The comparable effect that we observed on *psbT* translation in our experiments
774 (Figure 4) could be construed as evidence that this small polypeptide also belongs to
775 the PSII CES cascade. To our knowledge, no study has examined the possibility that
776 PsbT also is subject to translational regulation. To complicate the matter, RF-analysis
777 of the PSII mutant *nac2-26*, which lacks the D2 protein, rather showed a slight
778 increase in translation of *psbT* (Trösch et al., 2018). Because D1 itself (and hence all
779 the genes it controls via CES) needs D2 for full translation, the putative role of PsbT
780 in the CES cascade remains ambiguous. It should be noted that all three cistrons
781 belong to the conserved *psbB-T-H* operon and that the tetratricopeptide repeat
782 protein MBB1 is necessary for stabilization of the 5' end of the *psbB-psbT* mRNA as
783 well as the processing and translation of the co-transcribed *psbH* mRNA (Loizeau et

784 al., 2014; Vaistij et al., 2000). No monocistronic transcript has been described for
785 *PsbT*, so its CDS can only be translated from the *psbB-psbT* dicistronic mRNA
786 (Cavaiuolo et al., 2017; Monod et al., 1992). It is striking that the three ORFs that
787 depend on MBB1 for transcript stabilization or translation showed a strong reduction
788 of ribosome occupancy in the *ohp2* mutant (Figure 4C). This suggests a role for
789 MBB1 in the CES-regulation: it may work as a translation factor or recruit such a
790 factor. Even if MBB1 does not bind directly upstream of *psbT*, the increased
791 recruitment of the *psbB-psbT* transcript to ribosomes may enhance translation
792 initiation on *psbT*. Unfortunately, MBB1 could not be quantitated in our proteomic
793 analyses. The decrease in RF level observed over the *psbN* ORF which is positioned
794 between *psbT* and *psbH* but in antisense orientation could also indirectly involve
795 MBB1, if recruitment of the precursor *psbB-T-H* transcript to the polysomes affects
796 the stability/translatability of the antisense *psbN* mRNA. Coupling between
797 chloroplast mRNA stabilization and translation factors has been reported in
798 *Chlamydomonas*, for the MCA1/TCA1 couple. Changes in the abundance of
799 MCA1/TCA1 rapidly regulate *petA* mRNA accumulation and translation to meet the
800 cell's demand for synthesis of the CES-regulated *Cytf* subunit of the *Cytb_{6f}* complex
801 (Loiselay et al., 2008; Raynaud et al., 2007). Similarly, the abundance of TAA1,
802 involved in stabilization and translation of the *psaA* mRNA, has been reported to be
803 involved in the downregulation of PSI subunits upon iron deficiency (Lefebvre-
804 Legendre et al., 2015).

805 An unexpected result for the *ohp2* mutant in the RF experiment was the 2.8-fold
806 increase in RFs over *psbD*, encoding the main RC subunit D2 (Figures 4A, 4B;
807 Supplemental Figures S6B, S7; Supplemental Dataset 1). Because of the high
808 variability in the efficiency of ¹⁴C incorporation between strains and of the gel
809 background, we could not verify this by the pulse-labeling experiments (Figure 3C).
810 However, as all other D1 mutants studied thus far, like FuD7 or F35, completely
811 lacked D1 translation (Bennoun et al., 1986; Girard-Bascou et al., 1992; Yohn et al.,
812 1996), a stimulatory effect on D2 translation by the presence of unassembled D1 (as
813 possible in *ohp2*) could not have been observed. We note that translation of *psbD*
814 was not enhanced in any of the mutants studied by Chotewutmontri et al. (2020).

815 **The OHC is not completely essential for PSII biogenesis**

816 Another intriguing characteristic of the *Chlamydomonas ohp2* mutant is the high
817 frequency at which the non-photoautotrophic phenotype can be suppressed. A mere
818 plating on mineral medium, without any mutagenic treatment, was enough to
819 generate dozens of extragenic suppressors. In spite of all our efforts, we were unable
820 to identify a plausible causative variant, even though genetic analysis of three
821 independent suppressors indicated that the suppressor mutation(s) were tightly
822 linked, but unlinked to the *OHP2* or *FTSH1* loci. Furthermore, combination of *ohp2*
823 with the *ftsH1-1* mutation that severely affects activity of the FtsH protease (Malnoë
824 et al., 2014) allowed partial recovery of stable PSII charge separation, as revealed by
825 measurements of variable fluorescence and ECS (Figure 6C). This indicates that
826 whatever the exact action of the OHC on D1, it is not completely essential for
827 biogenesis of a functional PSII. A by-pass reaction must be possible, that leads to
828 partial restoration of PSII biogenesis. This pathway would be activated by the
829 suppressor mutation, but it probably already exists in the *ohp2* mutant: by slowing
830 down D1 degradation, the *ftsH1-1* mutation may allow a normally unstable form of D1
831 to proceed through this alternative pathway. It is probable that the PSII produced by
832 the alternative pathway is not fully functional, because the suppressed strains
833 showed some light-sensitivity, and the *ohp2 ftsH1-1* double mutant was not
834 photoautotrophic (Figure 6A). Alternatively, the activity of this alternative pathway
835 may be too low to allow efficient repair in high light. The *ftsH1-1* mutation by itself
836 renders the cell highly sensitive to photoinhibition. Detailed studies comparing PSII
837 purified from these strains may be necessary to answer this question.

838 **Consequences of the absence of OHP2 on other steps of the PSII assembly** 839 **pathway**

840 Based on the above, it was interesting to characterize the assembly intermediates in
841 the mutant and suppressor. We therefore used our proteomics data to monitor the
842 accumulation of the many PSII assembly factors described in the literature. Not only
843 did they represent candidate genes for the suppressor mutation, but changes in their
844 accumulation in the mutant and suppressor could reveal regulatory mechanisms at
845 play in *ohp2* and the suppressor. Some of the changes described below could be
846 brought about by regulation of gene expression, others by (de)stabilization of the

847 proteins. By comparing whole cells and membranes, we may also detect changes in
848 the association of these factors with PSII assembly intermediates, as recently
849 demonstrated by Spaniol et al. (2021) for the *lpa2* mutant. Figure 7 proposes a
850 working model for the role of the OHC and associated proteins in D1 synthesis,
851 combining previous reports from other organisms with data presented here for
852 *Chlamydomonas*. In the WT (Figure 7, left panel), HCF173 binds the 5'-UTR of *psbA*
853 mRNA to promote its translation (Link et al., 2012; Schult et al., 2007; Williams-
854 Carrier et al., 2019), which is then likely triggered by HCF244. Nascent pD1 protein is
855 co-translationally inserted into the thylakoid membrane where it is stabilized by
856 membrane-associated luminal HCF136. The OHC is proposed to further stabilize
857 pD1 by the insertion of Chl/Phe/Car, allowing its assembly in the RC complex and
858 formation of functional PSII core, dimer and finally supercomplexes. A striking result
859 of our targeted proteomics analysis was the two-fold overaccumulation of HCF173 in
860 the membranes of the *ohp2* mutant (Figure 5C, Supplemental Dataset 4). It was not
861 significantly overexpressed in the mutant at the whole cell level, so its increased
862 abundance in membranes probably indicates that a larger fraction of the *psbA* mRNA
863 is undergoing translation and thus found on membrane-associated polysomes. This
864 effect is no longer seen in the suppressor, suggesting that it is not a direct
865 consequence of the absence of the OHC, but rather a compensatory mechanism
866 caused by the PSII deficiency. As proposed above, unassembled D1 can no longer
867 regulate the activity of HCF244 in the mutant because the OHC cannot form
868 (Chotewutmontri et al., 2020; Link et al., 2012). This is expected to lead to enhanced
869 translation initiation on the *psbA* mRNA driven by the residual but fully active HCF244
870 (Figure 7, middle panel), unless a counteracting mechanism signals that PSII
871 biogenesis proceeds, as in the suppressor. SRRP1, another known interactant of
872 HCF173 and of the *psbA* mRNA, is believed to act as a repressor of translation
873 (Watkins et al., 2020). It could not be quantitated in the membranes, but interestingly,
874 while abundant in cells of the mutant and WT it was undetectable in the suppressor,
875 even though the gene appeared unaltered.

876 HCF136 is a conserved luminal protein, known in cyanobacteria as Ycf48. Its role
877 seems mostly to promote the association of the pD1/PsbI subcomplex with a distinct
878 precomplex consisting of D2 and the heterodimeric Cytb₅₅₉ (formed by the PsbE and
879 PsbF subunits), to form the RC (reviewed in Nickelsen and Rengstl, 2013; Zhang et
880 al., 1999). It is required for the assembly of early PSII intermediates, possibly with the

881 concurrent incorporation of Chl and has been found to bind pD1 (but not mature D1)
882 in a split-ubiquitin assay (Hey and Grimm, 2020; Knoppová et al., 2014; Komenda et
883 al., 2008; Li et al., 2019; Meurer et al., 1998; Myouga et al., 2018; Plücker et al.,
884 2002). It was therefore striking to observe that association of HCF136 with the
885 membrane (not its overall abundance) was markedly increased in the suppressor,
886 compared to the WT or mutant (Figure 5; Supplemental Datasets 2- 4). While
887 genome sequencing rules out *HCF136* as being the suppressor locus, its increased
888 abundance in the membranes of the suppressor may indicate the stabilization of a
889 complex comprising pD1, allowing it to associate with Chl via the alternative pathway
890 proposed above (Figure 7, right panel).

891 Assembly factors acting downstream of the formation of the RC can also be
892 impacted by the absence of OHP2. For example, the mutant did not show any
893 association of PSB28 with the membrane, consistent with the fact that this protein
894 binds to the RC47 complex (Zabret et al., 2021), that cannot form in the mutant. This
895 effect was reverted in the suppressor, in line with a restoration of the assembly
896 pathway. PSB27 binds to CP43 on the luminal surface of the PSII monomer and
897 dimer and contributes to the formation of the OEC (Avramov et al., 2020; Huang et
898 al., 2021; Zabret et al., 2021). In the *ohp2* mutant, it overaccumulates at the whole-
899 cell level, presumably through enhanced expression of the gene, but not in the
900 membranes, probably because of the absence of the RC. In contrast, the suppressor
901 showed enhanced binding of PSB27 to the membrane, suggesting that PSII formed
902 in the absence of the OHC requires prolonged association with PSB27, for example
903 because pD1 maturation, binding of the OEEs and/or photoactivation are delayed.
904 Another interesting observation that links back to the role of FtsH is the increased
905 association of PSB29/THF1 with the membrane in *ohp2*. The *Arabidopsis thf1* mutant
906 is variegated (Wang et al., 2004), a phenotype suppressed by mutations affecting
907 chloroplast gene expression (Hu et al., 2015; Zhang et al., 2009), just like that of the
908 *ftsH* mutants. THF1 is necessary for normal accumulation and function of FtsH in
909 land plants and cyanobacteria (Bečková et al., 2017; Huang et al., 2013; Zhan et al.,
910 2016). Its 3D structure has been solved (Bečková et al., 2017), but it is unclear yet
911 how it stabilizes or activates the protease. In our proteomic analysis, PSB29/THF1
912 was not over accumulated in any of the strains. However, its increased association
913 with the membrane in the mutant may reflect the increased activity of FtsH involved
914 in degrading ill-conformed D1.

915 **Other effects of the mutation in *OHP2* on chloroplast biogenesis**

916 Our RF experiments showed an increased translation of all the chloroplast-encoded
917 subunits of the ATP synthase in the *ohp2* mutant (Supplemental Figure S6,
918 Supplemental Dataset 1). Similarly, our proteomics experiments revealed an
919 increased abundance of all subunits of the complex (including the nucleus-encoded
920 ATPC/D/G), with a striking quantitative coherence in membrane samples (Figures 5A,
921 5B; Supplemental Datasets 2, 3). Increased levels of chloroplast ATP synthase
922 subunits were recently also observed in complexome profiling of the PSII-deficient
923 *lpa2* mutant from *Chlamydomonas* (Spaniol et al., 2021). Overaccumulation of the
924 ATP synthase could be involved in maintaining energy balance in the chloroplast: in
925 the absence of PSII, linear electron flow is abolished, but cyclic electron flow remains
926 possible between PSI and the *Cytb₆f* complex and generates a proton gradient that
927 can be used for ATP synthesis.

928 Our proteomics analysis showed increased accumulation of LHCI subunits in the
929 *ohp2* mutant, as well as in the suppressor strain. This suggests that the lack of OHP2
930 directly affects the biogenesis of PSI. Interestingly, BN-PAGE revealed a stronger
931 association of the PSI core and antenna subcomplexes in the mutant. This may be
932 related to the observation that the PSAN subunit, although not affected in whole cells,
933 was undetectable in the membranes of the mutant. In maize, PSAN lies at the
934 interface between the RC and LHCI (Pan et al., 2018), and this subunit was not
935 found in the structure of the *Chlamydomonas* PSI-LHCI complex (Suga et al., 2019),
936 suggesting that it modulates the association between the antenna and the RC in PSI.

937 Proteomics also revealed a general stimulation of the heme/Chl biosynthesis
938 pathway in the *ohp2* mutant (Figures 5A, 5B; Supplemental Datasets 2, 3). To our
939 knowledge, this is not a general feature of PSII deficient mutants and may be
940 specifically linked to the main purported function of OHP2/OHP1, i.e. integration of
941 Chl into a nascent polypeptide. Accumulation of the protochlorophyllide *a*
942 oxidoreductase POR1 was increased both at the cell and membrane level, while for
943 other enzymes like the Mg-chelatase, the Mg-protoporphyrin-IX methyltransferase
944 CHLM and the cyclase CTH1, the observed effect was an increased association with
945 the membrane. The OHC complex has been linked before with Chl synthesis, albeit
946 in different manners. In cyanobacteria, the Chl synthase ChlG (found unaffected here
947 in the *Chlamydomonas ohp2* mutant) co-immunoprecipitates with the homologs of
948 OHP2 and HCF244 (Chidgey et al., 2014). In the *Arabidopsis ohp2* mutant, Hey and

949 Grimm (2018) reported a decreased accumulation for most of the immunologically
950 analyzed Chl biosynthesis enzymes. The authors proposed a posttranslational
951 destabilization of these proteins in response to OHP2 deficiency, which could be
952 beneficial when D1, a major sink for newly synthesized Chl, is not translated. In
953 *Chlamydomonas*, the continued translation of D1, when the absence of OHP2 limits
954 its ability to ligate Chl, may instead start a signaling cascade aimed at increasing
955 production of Chl. The *ohp2* mutant may be missing a negative feedback loop
956 normally operating in the WT. For example, a product of the interaction between the
957 OHC and pD1, such as the Chl-associated but unassembled pD1, could negatively
958 regulate association of the Chl synthesis enzymes to the membrane, signaling that
959 more pD1 is made than can be assembled and the Chl flux should be lowered.
960 Similarly, the activity of HCF244 as a translation activator has been proposed to be
961 regulated by the interaction of pD1 with the OHC in the dark (Chotewutmontri and
962 Barkan, 2020). Another striking observation is the marked Chl deficiency in the
963 mutant (Supplemental Table S1). The PSII core contains 35 Chl *a* molecules, while
964 its pigment bed harbors ~200 Chl, so loss of the core itself cannot fully account for
965 the 40% decrease in Chl content that we observed. In the *Arabidopsis ohp2* mutants,
966 a comparable or even stronger reduction in Chl accumulation was observed, with Chl
967 *b* reduced to a lesser extent than Chl *a* (Hey and Grimm, 2018; Myouga et al., 2018).
968 A regulatory role of the OHC on Chl synthesis might be worth further exploration.

969 MATERIAL AND METHODS

970 Strains and culture conditions

971 The *ohp2* mutant (*10.1.a*) was isolated in a screen and was generated by nuclear
972 transformation of the mating type minus (mt-) cell-walled recipient strain Jex4 with the
973 plasmid pBC1 cut with *SacI* and *KpnI*, described in Houille-Vernes et al. (2011). For
974 backcrossing of *ohp2* strains, the wild type WT-S34 was used. For localization
975 studies the cell wall deficient *UVM4* strain generated by Neupert et al. (2009) was
976 used as recipient strain for glass bead transformation. Two PSII mutants, *nac2-26*
977 which lacks the *psbD* mRNA stabilization factor NAC2, and the *psbA* deletion mutant
978 FuD7, served as controls (Bennoun et al., 1986; Boudreau et al., 2000).

979 Algal strains were grown at 23°C under continuous white light on Tris-acetate-
980 phosphate medium (TAP) at ~10-20 $\mu\text{E}/\text{m}^2/\text{s}$, or on High Salt Minimum medium (MIN)

981 agar plates at 100 $\mu\text{E}/\text{m}^2/\text{s}$, respectively, if not indicated otherwise (Harris, 2009).
982 *ohp2* mutant strains were kept on plates at very low light ($\sim 5 \mu\text{E}/\text{m}^2/\text{s}$) to limit
983 inadvertent selection of suppressor mutants. Before usage of *ohp2* in experiments
984 the absence of potential PSII suppressors was confirmed by Fv/Fm measurements.
985 For experiments, liquid cultures of *Chlamydomonas* were grown in TAP medium
986 supplemented with 1% sorbitol (TAPS) at $\sim 20 - 30 \mu\text{E}/\text{m}^2/\text{s}$ until a cell density of 2-3
987 $\times 10^6$ cells/mL was reached.

988 The reversion rate of *ohp2*, was determined according to Kuras et al. (1997). *ohp2*
989 mutant cells were collected by centrifugation and resuspended in HSM to a density of
990 2×10^8 cells/mL. 0.5 mL was spread onto 10 HSM agar plates and maintained under
991 continuous light for three weeks, at which time colonies were counted.

992 **Spectroscopy and fluorescence measurements**

993 In vivo spectroscopy measurement using a JTS-10 spectrophotometer (Biologic,
994 Grenoble, France) was performed as described before in Jalal et al. (2015), using
995 cells grown under low light conditions. Fv/Fm is presented as the average of four
996 fluorescence induction measurements at 26, 56, 135 and 340 $\mu\text{E}/\text{m}^2/\text{s}$ followed by a
997 saturating pulse. PSII/PSI ratio was calculated from the difference in ECS signal at
998 520 nm, measured 160 μs after a saturating single turnover flash, in the absence or
999 presence of DCMU (10 μM) and hydroxylamine (1 mM) to measure (PSI+PSII) or PSI
1000 activity, respectively. In the latter condition, the b/a ratio is the ratio of amplitude of
1001 the second phase of the ECS signal (phase b, due to proton pumping by *Cytb₆f*) to
1002 the initial phase a (PSI) and is a rough measure of *Cytb₆f* activity.

1003 **Analysis of nucleic acids**

1004 For isolation of nucleic acids, cells were harvested by centrifugation at 1,100 x g, 4°C
1005 for 6 min. Genomic DNA was extracted using the DNeasy Plant Mini Kit (Qiagen,
1006 Hilden, Germany) according to manufacturer's protocol or CTAB buffer (2%
1007 cetyltrimethylammonium bromide, 100 mM Tris-HCl, pH 8) followed by
1008 phenol/chloroform/isoamyl alcohol extraction (25:24:1, Carl Roth GmbH, Mannheim,
1009 Germany). DNAs were digested by restriction enzymes and separated on 0.8%
1010 agarose gels set up in TPE-buffer (89 mM Tris-phosphate, 2 mM Na₂EDTA). Total
1011 cellular RNA was extracted by using the TRI reagent (Sigma-Aldrich, Saint Louis,

1012 USA), according to the manufacturer's instructions. RNAs were separated on 1%
1013 denaturing formaldehyde agarose gels. After separation nucleic acids were
1014 transferred to Roti Nylon⁺ membrane (Roth, Karlsruhe, Germany), followed by UV
1015 light cross-linking (UV Crosslinker, UVC 500, Hoefer Inc., San Francisco, USA). Dig-
1016 labeled probes were synthesized by PCR from total DNA or cloned cDNA (*psbA*) by
1017 using primers denoted in Supplemental Table S2. Hybridizations and detection of dig-
1018 labeled probes were performed using standard methods.

1019 **Immunoblot analysis**

1020 For isolation of total protein extracts, cells from 20 mL liquid cultures were harvested
1021 by centrifugation and cell pellets resuspended in 200 μ L 2 x lysis buffer (120 mM KCl,
1022 20 mM tricine pH 7.8, 5 mM β -mercaptoethanol, 0.4 mM EDTA, 0.2% Triton X100)
1023 supplemented with protease inhibitors (cOmplete[™] ULTRA Tablets, Mini, Roche,
1024 Switzerland) and lysed via sonication on ice. To separate membrane proteins from
1025 soluble proteins for cell subfractionation, cells from 50 mL culture were resuspended
1026 in 500 μ L hypotonic solution (10 mM Tricine/KOH pH 6.8, 10 mM EDTA, 5 mM β -
1027 mercaptoethanol, and protease inhibitors). Lysis was performed mechanically by
1028 vortexing thoroughly with glass beads (0.5 mm diameter) two times for 1 min. After
1029 centrifugation at 15,000 g for 10 min, the supernatant was considered as total soluble
1030 protein extract. The pellet containing the membrane proteins was resuspended in 2 \times
1031 lysis buffer.

1032 Protein concentration was measured by Bradford Protein Assay (Bradford, 1976).
1033 SDS-PAGE, protein gel blotting and immunodetection were performed as described
1034 by Sambrook and Russel (2001). Antibodies were as follows: α -PsaA (Agrisera,
1035 #AS06 172), α -D1 (Agrisera, #AS05084), α -CP43 (Agrisera, #AS11 1787) α -Cytf
1036 (Agrisera, # AS08 306), α -HA (Sigma-Aldrich, #H6908). The antiserum against the
1037 spinach Rubisco holoenzyme used for the detection of RbcL was kindly provided by
1038 G. F. Wildner (Ruhr-University Bochum). The antibody against the *Chlamydomonas*
1039 D2 protein was generated by immunization of rabbits using recombinant D2-GST
1040 protein (BioGenes GmbH, Berlin, Germany).

1041 **Complementation and localization studies**

1042 Constructs generated for the complementation of the *ohp2* mutant and OHP2
1043 localization studies are shown in Supplemental Figure S3. All constructs were
1044 created by the insertion of a PCR-amplified sequence of interest into the pBC1-
1045 CrGFP vector (= pJR38, Neupert et al., 2009; construct 1, Supplemental Figure S3)
1046 via NdeI or NdeI/EcoRI restriction sites. Primers used for cloning are given in
1047 Supplemental Table S2. For cloning details of the synthetic *Arabidopsis* gene
1048 (construct 6, Supplemental Figure S3) please see Supplemental Data S2. For
1049 localization studies, the cell wall deficient strain *UVM4* was transformed by the glass
1050 bead method (Kindle, 1990; Neupert et al., 2009) and positive transformants were
1051 selected by growth on TAP plates supplemented with 10 µg/mL paromomycin (Pm).
1052 For complementation, constructs were integrated into the genome of the *ohp2* mutant
1053 strain by the electroporation method (Shimogawara et al., 1998), selected for Pm
1054 resistance and subsequently screened for photoautotrophic growth on HSM plates.

1055 **2D blue native (BN) PAGE**

1056 500 mL liquid cultures of *Chlamydomonas* strains were harvested at 1,000 x g for 10
1057 min at 4°C and resuspended in 1 mL TMK buffer (10 mM Tris/HCl, pH 6.8, 10 mM
1058 MgCl₂, 20 mM KCl) and protease inhibitors (cOmplete™ ULTRA Tablets, Mini, Roche,
1059 Switzerland). Resuspended cells were lysed by sonication (ultrasound pulses of 10
1060 sec for 3 times). Cells were centrifuged (1,000 x g, 1 min, 4°C) to remove cell debris
1061 and unlysed cells. The supernatant was centrifuged for 10 min at 20,000 x g at 4°C.
1062 The resulting pellet was washed twice with TMK buffer and finally resuspended in
1063 500 µL TMK buffer. Chl concentration was determined by adding 20 µL of the sample
1064 to 980 µL methanol, 5 min incubation at RT and a 1 min centrifugation step to remove
1065 the starch. OD₆₅₂ of the supernatant was measured and Chl concentration
1066 calculated using the formula: Chl a (mg/mL) = A_{652nm} * 1.45. Aliquots containing 25
1067 µg of Chl were again centrifuged for 10 min, 20,000 g at 4°C and resuspended in 51
1068 µL ACA buffer (750 mM ε-aminocaproic acid, 50 mM Bis-Tris pH 7.0, 5 mM pH 7.0
1069 EDTA, 50 mM NaCl) and solubilized for 10 min on ice after addition of n-dodecyl-β-D-
1070 maltoside (β-DM) to a final concentration of 1.5%. Solubilized proteins were
1071 separated from insoluble material by centrifugation for 20 min, 16,000 x g at 4°C and
1072 mixed with 1/10 volume of BN loading dye (750 mM ε-aminocaproic acid, 5%

1073 Coomassie G250 (w/v)). First dimension native electrophoresis was carried out
1074 according to Schagger and Jagow (1991) on a 5 – 12 % linear gradient. Protein
1075 complexes were further subjected to 2D 12% SDS- PAGE and analyzed by
1076 immunoblotting.

1077 **Ribosome profiling and data analysis**

1078 For each replicate, 500 mL culture was supplemented with 100 µg/mL
1079 chloramphenicol and 100 µg/mL cycloheximide, followed by rapid cooling using
1080 plastic ice cubes. The cold (< 8°C) culture was then centrifuged at 3,000 g for 2 min
1081 to pellet the cells. The pellet was washed once with ice-cold polysome buffer (20 mM
1082 Tris pH 8.0, 25 mM KCl, 25 mM MgCl₂, 1 mM dithiothreitol, 100 µg/mL
1083 chloramphenicol, 100 µg/mL cycloheximide) and then flash-frozen in liquid nitrogen.
1084 The pellet was resuspended in 8 mL of polysome buffer containing 1x Protease
1085 inhibitor Cocktail (Roche) and 1 mM PMSF, and the cells were lysed using a French
1086 press (Avestin®) at 2 bar. Polysome isolation from the lysate, RNA digestion and FP
1087 isolation have been performed as described in Trosch et al. (2018). For the total
1088 RNA, a separate 8 mL of the culture was centrifuged at 3000 g for 2 min, and 750 µL
1089 of Trizol was added to the pellet directly. Total RNA extraction as well as RNA
1090 labelling and microarray analysis was performed as described in Trosch et al. (2018).

1091 Data processing and analysis was conducted according to previous studies
1092 (Trosch et al., 2018; Zoschke et al., 2013): Local background was subtracted from
1093 single channels (F635-B635 and F532-B532, respectively) and probes located within
1094 annotated and confirmed chloroplast reading frames were normalized to the average
1095 signal of the compared datasets including all replicates of ribosome FPs and total
1096 mRNA to remove overall differences introduced by technical variations. Probes
1097 covering a respective ORF were averaged, and relative abundance of ribosome FPs
1098 and total mRNA was calculated for each ORF by normalizing each ORF value to the
1099 average of all ORF values. By this, expression of the individual ORF is considered in
1100 relation to mean values of all plastid-encoded genes. Relative translation efficiency is
1101 determined by comparing to values of average FP intensities relative to the average
1102 RNA intensities, for each ORF. All average values and standard deviations are based
1103 on three independent biological replicates. Significant differences in gene-specific
1104 RNA and ribosome FP accumulation and translation efficiencies between WT and
1105 *ohp2* mutant data were determined with a Welch's t-test and corrected for multiple

1106 testing according to Storey's q-value method. Genes were marked as significant for
1107 q-value of <0.05 and with expression changes more than two-fold (Supplemental
1108 Dataset 1).

1109 **Mass spectrometry**

1110 Whole cell proteomics: 50 µg of proteins were separated by SDS-PAGE. After a short
1111 migration (< 0.5 cm) and Coomassie blue staining, gel bands containing proteins
1112 were excised and destained. Gel pieces were subjected to a 30 min reduction at
1113 56°C and a 1 h cysteine alkylation at room temperature using 10 mM dithiothreitol
1114 and 50 mM iodoacetamide in 50 mM ammonium bicarbonate, respectively. Proteins
1115 were digested overnight at 37°C using 500 ng of trypsin (Trypsin Gold, Promega).
1116 Supernatants were kept and peptides remaining in gel pieces were further extracted
1117 with 1% (v/v) trifluoroacetic acid. Corresponding supernatants were pooled and dried.
1118 Peptide mixtures were subsequently reconstituted in 200 µL of solvent A (0.1% (v/v)
1119 formic acid in 3% (v/v) acetonitrile). Five microliters of peptide mixtures were
1120 analyzed in duplicate on a Q-Exactive Plus hybrid quadrupole-orbitrap mass
1121 spectrometer (Thermo Fisher) as described in Pérez-Pérez et al. (2017) except that
1122 peptides were separated on a PepMap™ RSLC C18 Easy-Spray column (75 µm x 50
1123 cm, 2 µm, 100 Å; Thermo Scientific) with a 90 min gradient (0 to 20% B solvent (0.1%
1124 (v/v) formic acid in acetonitrile) in 70 min and 20 to 37% B solvent in 20 min).

1125 Membrane proteomics: Cells were collected by centrifugation, resuspended in 25
1126 mM phosphate buffer at a density of app. 0.5 µg/µL total Chl and disrupted by three
1127 consecutive freeze and thaw cycles. Soluble proteins were separated by
1128 centrifugation at 4°C, 25,000 g for 15 min. 20 µg total protein from the pellet fraction
1129 were precipitated in 80 % acetone, tryptically digested and desalted as described
1130 (Hammel et al., 2018). Peptides were resuspended in a solution of 2% acetonitrile,
1131 1% formic acid just before the LC-MS/MS run. The LC-MS/MS system (Eksigent
1132 nanoLC 425 coupled to a TripleTOF 6600, ABSciex) was operated basically as
1133 described for data dependent acquisition (Hammel et al., 2018).

1134 For targeted MRM-HR data acquisition a list of 39 precursor m/z was chosen for
1135 targeting the 5 different proteins. The precursors were selected from results of the
1136 data dependent acquisitions and good responding peptides as predicted by a deep
1137 learning algorithm for peptide detectability prediction, d::pPop (Zimmer et al., 2018).
1138 Collision energies were calculated from the standard CE parameters of the

1139 instrument, dwell time was set to 60 ms, fragments were acquired from 110 m/z –
1140 1600 m/z, resulting in a cycle time of 2.6 s.

1141 *Data processing and label-free quantification.* Shotgun proteomics raw data were
1142 processed using the MaxQuant software package as described in Martins et al.
1143 (2020) with slight modifications. For protein identification and target decoy searches
1144 were performed using a home-made *Chlamydomonas reinhardtii* protein database
1145 consisting in the JGI Phytozome nuclear-encoded proteins database (v.5.6)
1146 concatenated with chloroplast- and mitochondria-encoded proteins in combination
1147 with the Maxquant contaminants.

1148 For whole cell proteomics the mass tolerance in MS and MS/MS was set to 10
1149 ppm and 20 mDa, respectively and proteins were validated if at least 2 unique
1150 peptides having a protein FDR < 0.01 were identified. For quantification, unique and
1151 razor peptides with a minimum ratio count ≥ 2 unique peptides were used and protein
1152 intensities were calculated by Delayed Normalization and Maximal Peptide Ratio
1153 Extraction (MaxLFQ) according to Cox et al. (2014). For membrane protein data
1154 dependent runs MaxQuant software (v1.6.0.1) (Cox and Mann, 2008; Tyanova et al.,
1155 2016) was used. Peptide identification, protein group assignment and quantification
1156 was done with standard settings for ABSciex Q-TOF data except that 3 miss-
1157 cleavages were allowed, minimum peptide length was set to 6 AA, maximum peptide
1158 mass 6600 Da.

1159 *Shotgun data analysis:* For statistical analysis, LFQ intensities obtained from
1160 MaxQuant were further analyzed with the Perseus software package version 1.6.15.0
1161 (Tyanova et al., 2016). In case of the whole cell data the two measurement replicates
1162 were averaged first. For both datasets the biological replicates were grouped and the
1163 LFQ intensities were Log_2 transformed. The data were filtered to contain at least
1164 three valid values (out of four biological replicates) or two valid values (out of three
1165 biological replicates) in case of the whole cell or membrane fractions, respectively.
1166 Significant changes in LFQ intensities compared to the WT were identified by a
1167 modified two sample t-test of the Perseus software (permutation-based FDR=5%,
1168 artificial within group variance $S_0=1$). The *ohp2* mutant, the suppressor mutant *M-su1*
1169 and in case of the whole cell samples the complemented line *ohp2:OHP2-HA*, were
1170 compared to the WT independently. Data visualizations shown in Figure 5 and
1171 Supplemental Figure S9 were done using R (R Core Team, 2018). The log_2
1172 transformed LFQ intensities and t-test results of the whole cell samples and

1173 membrane fractions are shown in Supplemental Dataset 2 and Supplemental Dataset
1174 3, respectively.

1175 *Targeted mass spectrometry data analysis* was done using Skyline software
1176 (v20.1.0.155) (MacLean et al., 2010; Pino et al., 2020). The spectral library was built
1177 by prediction using Prosit (Gessulat et al., 2019), retention times were taken, where
1178 possible, from identification results of the respective peptides using MaxQuant. A
1179 minimum of 2 precursors per protein and 4 transitions per precursor was used for
1180 quantification. The integration borders were manually adjusted where necessary and
1181 dotp values for the coeluting fragments as reported from Skyline was taken as a
1182 quality measure for correct assignment (Supplemental Dataset 4). Retention times
1183 varied over all runs by less than 0.5 min, dotp values were usually >0.85 across the
1184 replicates where a correct assignment was assumed. Summed fragment peak areas
1185 were normalized for unequal sample loading to the total intensities of proteins as
1186 identified by MaxQuant in data dependent runs.

1187 The untargeted mass spectrometry proteomics data have been deposited to the
1188 ProteomeXchange Consortium via the PRIDE (Perez-Riverol et al., 2021) partner
1189 repository with the dataset identifier PXD031558 (**Reviewer account details:**
1190 **<https://www.ebi.ac.uk/pride/login>; Username: reviewer_pxd031558@ebi.ac.uk;**
1191 **Password: D3xVDFGU**). The targeted mass spectrometry proteomics data have
1192 been deposited to the ProteomeXchange Consortium via the Panorama Public
1193 (Sharma et al., 2018) partner repository with the dataset identifier PXD031631
1194 (**Reviewer account details: <https://panoramaweb.org/TIFMYS.url>; Username:**
1195 **panorama+reviewer102@proteinms.net; Password: iEqMdcRZ**).

1196 **FUNDING**

1197 We gratefully acknowledge financial support from the Deutsche
1198 Forschungsgemeinschaft to JN (Grants Ni390/7-1 and TRR175-A06), AVB (Grant BO
1199 4686/1-1), FWi (TRR 175-A05), MS (TRR 175-C02) and from the CNRS (UMR7141)
1200 and LABEX DYNAMO (ANR-11-LABX-0011-01) to OV. Further support to the
1201 Proteomic Platform of IBPC (PPI) was provided by EQUIPEX (CACSI ANR-11-
1202 EQPX-0008). FWa was supported by the Chinese Scholarship Council (CSC).

1203 **AUTHOR CONTRIBUTIONS**

1204 AVB, OVA, FWi, JN, and MS conceived and designed the research; FWa, KD, IM,
1205 FE, RT, FS, OVA, AVB, and XJ performed the experiments; FS, LDW, and FWi
1206 analyzed data; AVB, OVA, and FWi wrote the paper with inputs from all authors.

1207 **ACKNOWLEDGEMENTS**

1208 The authors would like to thank C. de Vitry for providing the *ftsH1-1* strain.

1209 **FIGURE LEGENDS**

1210 **Figure 1. Identification and complementation of the mutation in *OHP2*.**

1211 **A)** Schematic representation of the genomic region of *OHP2* (*Cre06.g251150*) on
1212 chromosome 6. Grey boxes indicate exons, smaller grey arrow and box 5' and 3'
1213 UTRs, respectively, and light grey boxes introns. For simplicity, upstream and
1214 downstream loci are not displayed. The probe used in B) is shown as black bar
1215 above the gene model. The insertion site of a putative >5 kb *TOC1* transposon in
1216 exon 3 of the *OHP2* gene in the mutant strain *10.1a* is indicated by an open triangle
1217 (compare Supplemental Figure S2). The filled black triangle in intron 2 of the *OHP2*
1218 gene indicates the position of a polymorphism caused by an additional putative
1219 insertion in the mutant and its background strain as identified during Illumina
1220 sequencing (compare Supplemental Figure S2). Given position of HindIII (H) and PstI
1221 (P) restriction sites are based on the reference genome of *Chlamydomonas*
1222 *reinhardtii* v5.5 in Phytozome. Note that this sequence is based on the mt+ genome
1223 assembly of strain *CC-503* and does not necessarily reflect the restriction site
1224 positions in the investigated mt- allele. **B)** Southern blot analysis of genomic DNA
1225 from the Jex4 recipient strain (WT) and the *10.1a* mutant. 10 µg of genomic DNA
1226 were fractionated in a 0.8% agarose gel after digestion by restriction enzymes HindIII
1227 or PstI, respectively, blotted onto a nylon membrane, and hybridized with the *OHP2*-
1228 specific probe indicated in A). **C)** Photosynthetic parameters of the Jex4 recipient
1229 strain (WT), the *ohp2* mutant and *ohp2* complemented with pBC1-CrOHP2-HA
1230 (*ohp2:OHP2-HA*, compare construct 2 in Supplemental Figure S3). Fluorescence
1231 induction kinetics (upper panel), measured under illumination at 135 µE/m²/s,
1232 followed by a saturating pulse (arrow) and dark relaxation. Fluorescence intensity is
1233 normalized to the F_m value. Electrochromic shift at 520 nm (lower panel), measured

1234 in the absence or presence of DCMU and hydroxylamine. Values are normalized to
1235 the signal after the saturating flash. **D)** Growth test. Cells were resuspended in sterile
1236 H₂O to a concentration of 10⁵ cells/mL and spotted onto acetate-containing (TAP) or
1237 High Salt Minimum media (MIN) and grown for 6 d under higher light (HL) at 100
1238 $\mu\text{E}/\text{m}^2/\text{s}$ or low light (LL) at 30 $\mu\text{E}/\text{m}^2/\text{s}$.

1239 **Figure 2. Protein sequence alignment and complementation analysis.**

1240 **A)** Sequence alignment of eukaryotic One-Helix Proteins OHP1 and OHP2 and two
1241 cyanobacterial HLIPs. OHP2 and OHP1 protein sequences from C.r. (*C. reinhardtii*,
1242 v5.5, *Cre06.g251150* and *Cre02.g109950*), A.t. (*Arabidopsis thaliana*, TAIR10,
1243 *AT1G34000.1* and *AT5G02120*), P.p. (*Physcomitrella patens*, v3.3,
1244 Pp3c2_26700V3.1), and Z.m. (*Zea mays*, PH207 v1.1, Zm00008a032025_T01) were
1245 obtained from Phytozome (<https://phytozome.jgi.doe.gov/pz/portal.html>). Amino acid
1246 sequences of the High light-induced proteins HliC (*ssl1633*) and HliD (*ssr1789*) from
1247 *Synechocystis* sp. PCC6803 were taken from CyanoBase
1248 (<http://www.kazusa.or.jp/cyano/>). The multiple sequence alignment was performed by
1249 using ClustalW (Thompson et al., 2002), manually edited and displayed with
1250 Genedoc (Nicholas et al., 1997). Black shading represents 100% conservation, dark
1251 grey and grey 60% and 40%, respectively. The positions of the predicted Chl binding
1252 region as well as a hydrophobic stretch (HS) at the C-terminus are indicated
1253 (compare Supplemental Figure S4A). Two residues described to be important for Chl
1254 binding in LHCB from spinach are labeled with red asterisks (Kühlbrandt et al., 1994).
1255 The N-terminal chloroplast transit peptides predicted by TargetP-2.0 (Emanuelsson et
1256 al., 2000; Nielsen et al., 1997) for all eukaryotic proteins shown, are not included in
1257 the alignment. The *Chlamydomonas* OHP2-based prediction of a transmembrane
1258 helix by TMPred (Hofmann and Stoffel, 1993; [https://embnet.vital-](https://embnet.vital-it.ch/software/TMPRED_form.html)
1259 [it.ch/software/TMPRED_form.html](https://embnet.vital-it.ch/software/TMPRED_form.html)), is indicated as a grey bar above the sequence
1260 (compare Supplemental Figure S4B). The mutation identified in the *Chlamydomonas*
1261 *OHP2* gene corresponds to residue M76 of the protein (indicated by a red triangle)
1262 which lies within the fully-conserved stretch in the N-terminal part of the protein. **B)**
1263 The C-terminal hydrophobic stretch is required for restoration of photoautotrophy.
1264 Growth test (left panel). The *ohp2* mutant was transformed with the construct pBC1-
1265 CrOHP2- Δ HS-HA (see construct 5 in Supplemental Figure S3). Pm-resistant
1266 transformants (*ohp2:CrOHP2- Δ HS-HA*) were tested for photoautotrophic growth on

1267 HSM plates (MIN). Immunoblot analysis (right panel) of Pm-resistant transformants.
1268 40 µg of total proteins were separated on 15% denaturing polyacrylamide gels and
1269 analyzed with the antibodies indicated on the left. The complemented strain
1270 *ohp2:OHP2-HA* was used as positive control for the accumulation of HA-tagged
1271 proteins. Samples were run on the same gel but not in adjacent lanes as indicated by
1272 a vertical black line.

1273 **Figure 3. Drastically diminished D1 protein accumulation and synthesis in the**
1274 ***ohp2* mutant.**

1275 The following strains were subjected to analysis: Jex4 (WT), *ohp2* and the
1276 complemented strain *ohp2:OHP2-HA* clone #53 (*ohp2:OHP2-HA*). **A)** Accumulation
1277 of photosynthesis related chloroplast proteins. 30 µg of total proteins from indicated
1278 strains were separated by 12% (α-D1, α-PsaA, α-Cytf, α-CP43, α-D2) or 15% (α-HA,
1279 α-RbcL) denaturing polyacrylamide gels and analyzed by the antibodies indicated. **B)**
1280 Accumulation of photosynthesis related chloroplast transcripts. 3 µg of total cellular
1281 RNA from indicated strains were fractionated by denaturing agarose gel
1282 electrophoresis and blotted onto a nylon membrane. Membranes were hybridized
1283 with probes specific for *psbA* and *psbD*. For loading control, the same blot was
1284 hybridized with a probe specific for *rbcL* transcripts. *nac2* and *FuD7* mutants were
1285 employed as negative controls for *psbD* or *psbA* mRNA accumulation, respectively.
1286 *ohp2* was run on the same gel but not in adjacent lanes as indicated by a vertical
1287 black line. **C)** Synthesis of PSII subunits. ¹⁴C labelling of chloroplast-encoded
1288 proteins was performed as described previously in Spaniol et al. (2021).
1289 Autoradiogram of cells pulsed for 5 min with ¹⁴C-acetate in the presence of
1290 cycloheximide (left), then chased for 45 min after washing and chloramphenicol
1291 addition. For *ohp2*, two independently grown cultures (#1, #2) were analyzed. The
1292 complemented strain was run on the same gel and exposed in the same conditions,
1293 but in non-adjacent lanes as indicated by a vertical black line. **D)** 2D BN-PAGE
1294 analysis of photosynthetic protein complexes in indicated strains. After solubilization
1295 of membranes with 1.5% (w/v) dodecyl-b-D-maltopyranoside, thylakoid proteins were
1296 separated by 5 to 12 % BN gels in the first dimension and 12% SDS-gels in the
1297 second dimension. Photosynthetic complexes were detected using the indicated
1298 antibodies. The positions of major PSI and PSII complexes are designated. sc:
1299 supercomplex

1300 **Figure 4. Targeted ribosome profiling of chloroplast translation reveals protein**
1301 **synthesis defects in the *ohp2* mutant.**

1302 Ribosome profiling and transcript analysis of WT and *ohp2* mutant grown
1303 mixotrophically under 30 $\mu\text{E}/\text{m}^2/\text{s}$. **A)** The average mRNA (blue) and ribosome FP
1304 (dark grey) abundances were calculated from three independent biological replicates
1305 and plotted in \log_{10} scale for *ohp2* mutant versus WT, respectively. mRNAs encoding
1306 PSII subunits, which display altered translation in the mutant are highlighted.
1307 *Pearsons's* *r*-value and *p*-value are given in *nEm* non-superscript format for *n*•10*m*.
1308 **B)** The relative average transcript abundances (RNA), translation output and
1309 translation efficiency were calculated for each chloroplast reading frame in both
1310 *Chlamydomonas* strains, normalized to overall signal intensities, and plotted as heat
1311 map (*ohp2* versus WT) in \log_2 scale. Increased RNA accumulation, translation output
1312 or translation efficiency in the mutant is shown in red, reduced levels are shown in
1313 blue (see scale bar). PSII subunits that are further discussed are highlighted with an
1314 arrow. **DC)** For the Open Reading Frames (ORFs) of *psbA* (introns not shown) and
1315 the *psbB* operon normalized ribosome FP intensities were plotted as mean \log_2 ratios
1316 between *ohp2* mutant and WT. Error bars denote differences between three
1317 independent biological replicates. Grey bars below the panels indicate respective
1318 ORFs with trans-membrane segments (TMS in green). Related to Supplemental
1319 Figures S6, S7 and Supplemental Dataset 1. **D)** CES cascade of PSII. When newly
1320 synthesized CES polypeptides, like D1 and CP47, cannot assemble, they repress the
1321 translation initiation of their encoding mRNA as described before by Minai and
1322 coworkers (2006). Reduced translation of *psbH* may indicate that it represents a
1323 further component of the CES cascade.

1324 **Figure 5. Altered proteome composition in the *ohp2* mutant and suppressor**
1325 **strain.**

1326 Volcano plots representing the relative proteome changes of whole cell lysates (**A)** of
1327 *ohp2* mutants versus WT (left), suppressor line 1 versus WT (right) and thylakoid
1328 membrane proteins (**B)** as comparison between *ohp2* mutant versus WT (left) and
1329 suppressor line 1 versus WT (right). For B), proteins of the membrane fraction were
1330 enriched by crude fractionation. All experiments were performed in at least three
1331 independent biological replicates. Mean fold change of LFQ values (in \log_2) is plotted

1332 on the x-axis, p -values (in $-\log_{10}$) are plotted on the y-axis. Light grey dots represent
1333 proteins with no significant change, dark grey dots show proteins that are significantly
1334 different with $FDR < 0.05$ and $S_0=1$. Proteins of PSI, PSII, the chloroplast ATP
1335 synthase, and of proteins involved in Chl biogenesis are marked in color as depicted
1336 in the legend on the right. Large colored dots are significantly different. **C)** Abundance
1337 of selected proteins in membrane protein extracts as determined by targeted mass
1338 spectrometry in different strains as compared to WT. Error bars indicate standard
1339 deviation over three biological replicates. Missing values indicate instances where no
1340 peptides could be found or are present below baseline signal of app. 5% compared
1341 to WT as judging from dotp values and fragment coelution profiles. Related to
1342 Supplemental Figure S9 and Supplemental Datasets 2-4.

1343 **Figure 6. Mutation of the FtsH protease partially restores PSII activity but not**
1344 **photoautotrophy.**

1345 **A)** Growth tests of the progeny of a cross *10.1a X ftsH1-1*. Cells were grown on TAP
1346 or MIN medium at the indicated light intensity. Spots shown are typical of the
1347 indicated genotypes. **B)** Fv/Fm values for the four genotypes, recorded from the
1348 plates in A). Values are average of 8, 7, 11 and 6 strains for the WT, *ftsH1*, *ohp2* and
1349 *ohp2 ftsH1* genotypes, respectively. Error bars represent S.D. **C)** Typical
1350 fluorescence induction curves for the four genotypes, recorded with the fluorescence
1351 camera on the TAP plates described in A). Fluorescence is normalized to the Fm
1352 value (arrow indicates saturating flash).

1353 **Figure 7. Schematic model for the role the OHC complex and associated**
1354 **proteins in D1 synthesis and first steps of PSII de novo assembly.**

1355 In the WT (**left panel**), likely triggered by HCF244, HCF173 binds the 5'-UTR of *psbA*
1356 mRNA to promote translation initiation. pD1 is co-translationally inserted into the
1357 thylakoid membrane. Membrane associated luminal HCF136 stabilizes pD1 and is
1358 involved in RC assembly. The OHC is required for early PSII assembly steps and
1359 proposed to insert Chl into pD1 proteins. Recently reported negative autoregulatory
1360 circuits of *psbA* translation initiation involving the OHC are not displayed here
1361 (Chotewutmontri and Barkan, 2020; Chotewutmontri et al., 2020). In *ohp2* (**middle**
1362 **panel**) and suppressor strains (**right panel**) residual levels of HCF244 may promote

1363 *psbA* translation via interaction with HCF173. Ongoing *psbA* translation may be
1364 further supported by overaccumulation of HCF173. However, in the *ohp2* mutant
1365 synthesized D1 is rapidly degraded and does not accumulate in the absence of the
1366 OHC complex. In the suppressor strains, stabilization of nascent D1 may be
1367 accomplished by increased membrane association of HCF136 or other mechanisms
1368 to allow assembly of early PSII intermediates. HCF173, HCF136, and HCF244
1369 protein amounts detected by proteomics are indicated by differently sized ovals.
1370 Names of cyanobacterial homologs are given in brackets.

1371 **SUPPLEMENTAL MATERIAL**

1372 **SUPPLEMENTAL FIGURES**

1373 **Figure S1.** Genetic analysis of the *10.1a* mutant.

1374 **Figure S2.** Identification of the *ohp2* mutation.

1375 **Figure S3.** DNA constructs used for complementation and localization studies.

1376 **Figure S4.** Hydrophobicity prediction for *Chlamydomonas* and *Arabidopsis* OHP2
1377 amino acid sequences.

1378 **Figure S5.** OHP2 is a membrane localized chloroplast protein.

1379 **Figure S6.** Reproducibility of RF experiments and results for all chloroplast encoding
1380 genes.

1381 **Figure S7.** Targeted ribosome profiling of chloroplast translation reveals enhanced
1382 *psbD* translation in the *ohp2* mutant.

1383 **Figure S8.** Re-accumulation of D2 and restoration of photoautotrophy in suppressor
1384 mutants.

1385 **Figure S9.** Heat maps representing the reproducibility of LC-MS experiments and
1386 complementation of *ohp2*.

1387 **Figure S10.** Complementation of the *ohp2* mutant with the orthologous *Arabidopsis*
1388 protein restores photoautotrophy and D1 accumulation.

1389 **Figure S11.** Transcript accumulation level of *OHP2*, *OHP1*, and HCF244 in
1390 *Chlamydomonas* under various growth conditions.

1391 **SUPPLEMENTAL TABLES AND DATA**

1392 **Supplemental Table S1.** Photosynthetic parameters and Chl composition of
1393 *Chlamydomonas* WT Jex4 (WT), the *ohp2* mutant and complemented strain.

1394 **Supplemental Table S2.** Primers used in this study.

1395 **Supplemental Data S1.** Flanking sequence tags in the *ohp2* mutant obtained by
1396 Illumina sequencing.

1397 **Supplemental Data S2.** Synthetic *Arabidopsis OHP2* nucleotide sequences and
1398 derived protein sequence used to complement the *Chlamydomonas ohp2* mutant
1399 strain.

1400 **SUPPLEMENTAL DATASETS**

1401 **Supplemental Dataset 1.** Complete dataset from array-based ribosome profiling
1402 experiments.

1403 **Supplemental Dataset 2.** Complete dataset from whole cell proteomics experiments.

1404 **Supplemental Dataset 3.** Complete dataset from membrane proteomics
1405 experiments.

1406 **Supplemental Dataset 4.** Targeted mass spectrometry data

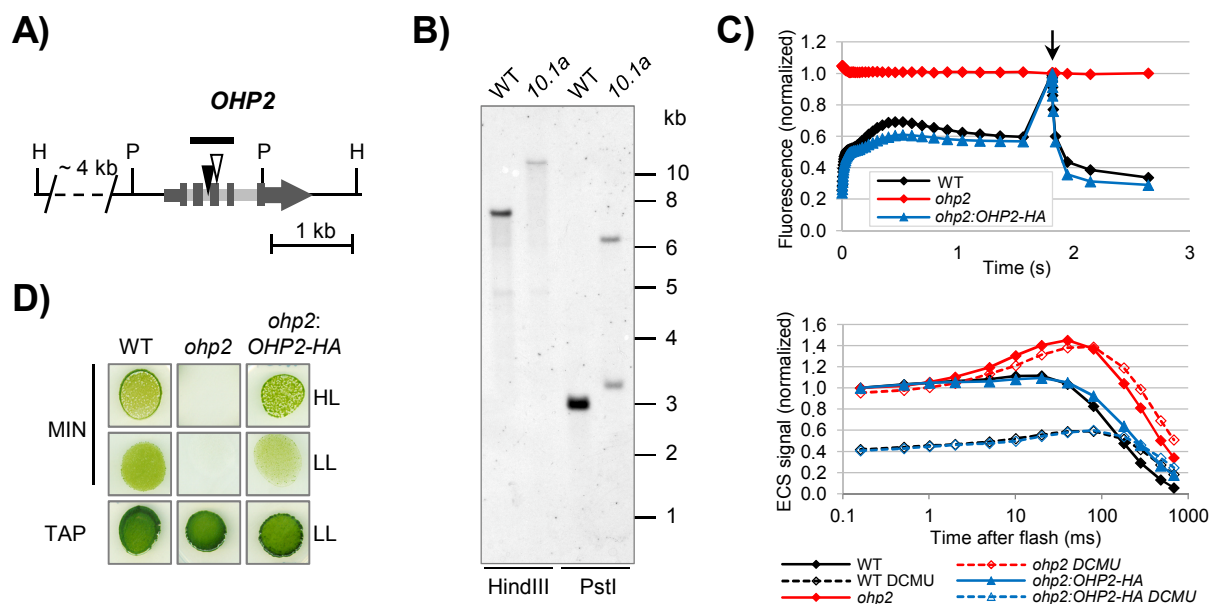


Figure 1. Identification and complementation of the mutation in *OHP2*. **A)** Schematic representation of the genomic region of *OHP2* (*Cre06.g251150*) on chromosome 6. Grey boxes indicate exons, smaller grey arrow and box 5' and 3' UTRs, respectively, and light grey boxes introns. For simplicity, upstream and downstream loci are not displayed. The probe used in B) is shown as black bar above the gene model. The insertion site of a putative >5 kb *TOC1* transposon in exon 3 of the *OHP2* gene in the mutant strain *10.1a* is indicated by an open triangle (compare Supplemental Figure S2). The filled black triangle in intron 2 of the *OHP2* gene indicates the position of a polymorphism caused by an additional putative insertion in the mutant and its background strain as identified during Illumina sequencing (compare Supplemental Figure S2). Given position of HindIII (H) and PstI (P) restriction sites are based on the reference genome of *Chlamydomonas reinhardtii* v5.5 in Phytozome. Note that this sequence is based on the mt+ genome assembly of strain CC-503 and does not necessarily reflect the restriction site positions in the investigated mt- allele. **B)** Southern blot analysis of genomic DNA from the Jex4 recipient strain (WT) and the *10.1a* mutant. 10 μ g of genomic DNA were fractionated in a 0.8% agarose gel after digestion by restriction enzymes HindIII or PstI, respectively, blotted onto a nylon membrane, and hybridized with the *OHP2*-specific probe indicated in A). **C)** Photosynthetic parameters of the Jex4 recipient strain (WT), the *ohp2* mutant and *ohp2* complemented with pBC1-CrOHP2-HA (*ohp2:OHP2-HA*, compare construct 2 in Supplemental Figure S3). Fluorescence induction kinetics (upper panel), measured under illumination at 135 μ E/m²/s, followed by a saturating pulse (arrow) and dark relaxation. Fluorescence intensity is normalized to the Fm value. Electrochromic shift at 520 nm (lower panel), measured in the absence or presence of DCMU and hydroxylamine. Values are normalized to the signal after the saturating flash. **D)** Growth test. Cells were resuspended in sterile H₂O to a concentration of 10⁵ cells/mL and spotted onto acetate-containing (TAP) or High Salt Minimum media (MIN) and grown for 6 d under higher light (HL) at 100 μ E/m²/s or low light (LL) at 30 μ E/m²/s.

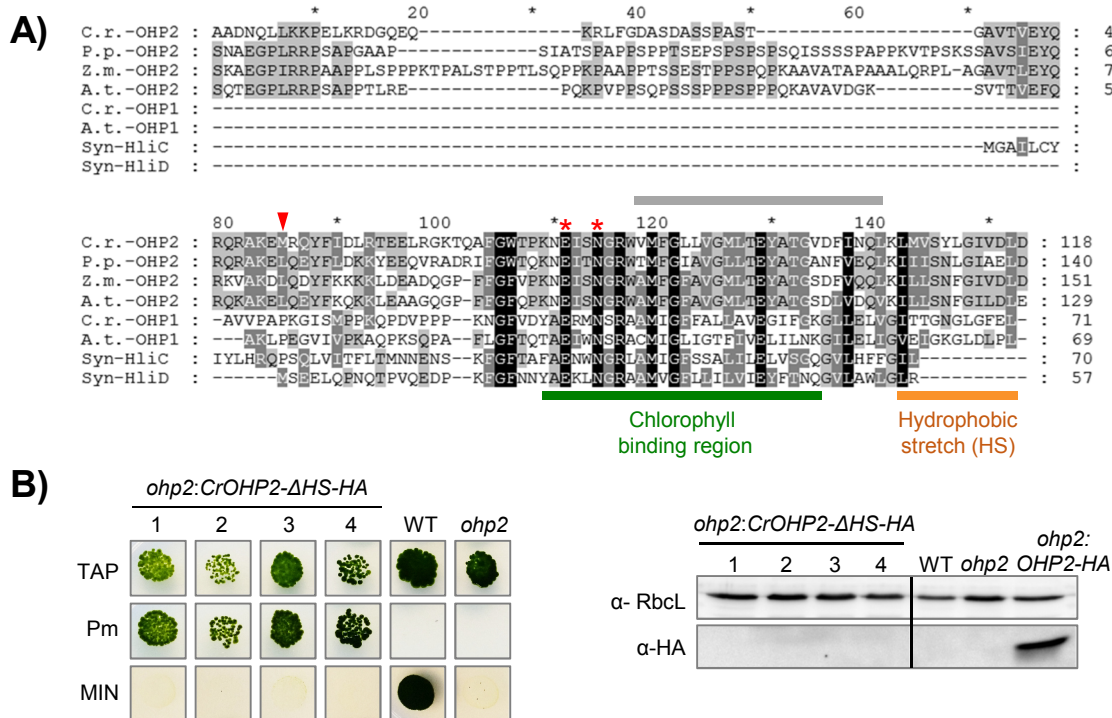


Figure 2. Protein sequence alignment and complementation analysis. **A)** Sequence alignment of eukaryotic One-Helix Proteins OHP1 and OHP2 and two cyanobacterial HLIPs. OHP2 and OHP1 protein sequences from C.r. (*C. reinhardtii*, v5.5, *Cre06.g251150* and *Cre02.g109950*), A.t. (*Arabidopsis thaliana*, TAIR10, *AT1G34000.1* and *AT5G02120*), P.p. (*Physcomitrella patens*, v3.3, *Pp3c2_26700V3.1*), and Z.m. (*Zea mays*, PH207 v1.1, *Zm00008a032025_T01*) were obtained from Phytozome (<https://phytozome.jgi.doe.gov/pz/portal.html>). Amino acid sequences of the High light-induced proteins HliC (*ssl1633*) and HliD (*ssl1789*) from *Synechocystis* sp. PCC6803 were taken from CyanoBase (<http://www.kazusa.or.jp/cyano/>). The multiple sequence alignment was performed by using ClustalW (Thompson et al., 2002), manually edited and displayed with Genedoc (Nicholas et al., 1997). Black shading represents 100% conservation, dark grey and grey 60% and 40%, respectively. The positions of the predicted Chl binding region as well as a hydrophobic stretch (HS) at the C-terminus are indicated (compare Supplemental Figure S4A). Two residues described to be important for Chl binding in LHCb from spinach are labeled with red asterisks (Kühlbrandt et al., 1994). The N-terminal chloroplast transit peptides predicted by TargetP-2.0 (Emanuelsson et al., 2000; Nielsen et al., 1997) for all eukaryotic proteins shown, are not included in the alignment. The *Chlamydomonas* OHP2-based prediction of a transmembrane helix by TMPred (Hofmann and Stoffel, 1993; https://embnet.vital-it.ch/software/TMPRED_form.html), is indicated as a grey bar above the sequence (compare Supplemental Figure S4B). The mutation identified in the *Chlamydomonas* OHP2 gene corresponds to residue M76 of the protein (indicated by a red triangle) which lies within the fully-conserved stretch in the N-terminal part of the protein. **B)** The C-terminal hydrophobic stretch is required for restoration of photoautotrophy. Growth test (left panel). The *ohp2* mutant was transformed with the construct pBC1-CrOHP2-ΔHS-HA (see construct 5 in Supplemental Figure S3). Pm-resistant transformants (*ohp2:CrOHP2-ΔHS-HA*) were tested for photoautotrophic growth on HSM plates (MIN). Immunoblot analysis (right panel) of Pm-resistant transformants. 40 μg of total proteins were separated on 15% denaturing polyacrylamide gels and analyzed with the antibodies indicated on the left. The complemented strain *ohp2:OHP2-HA* was used as positive control for the accumulation of HA-tagged proteins. Samples were run on the same gel but not in adjacent lanes as indicated by a vertical black line.

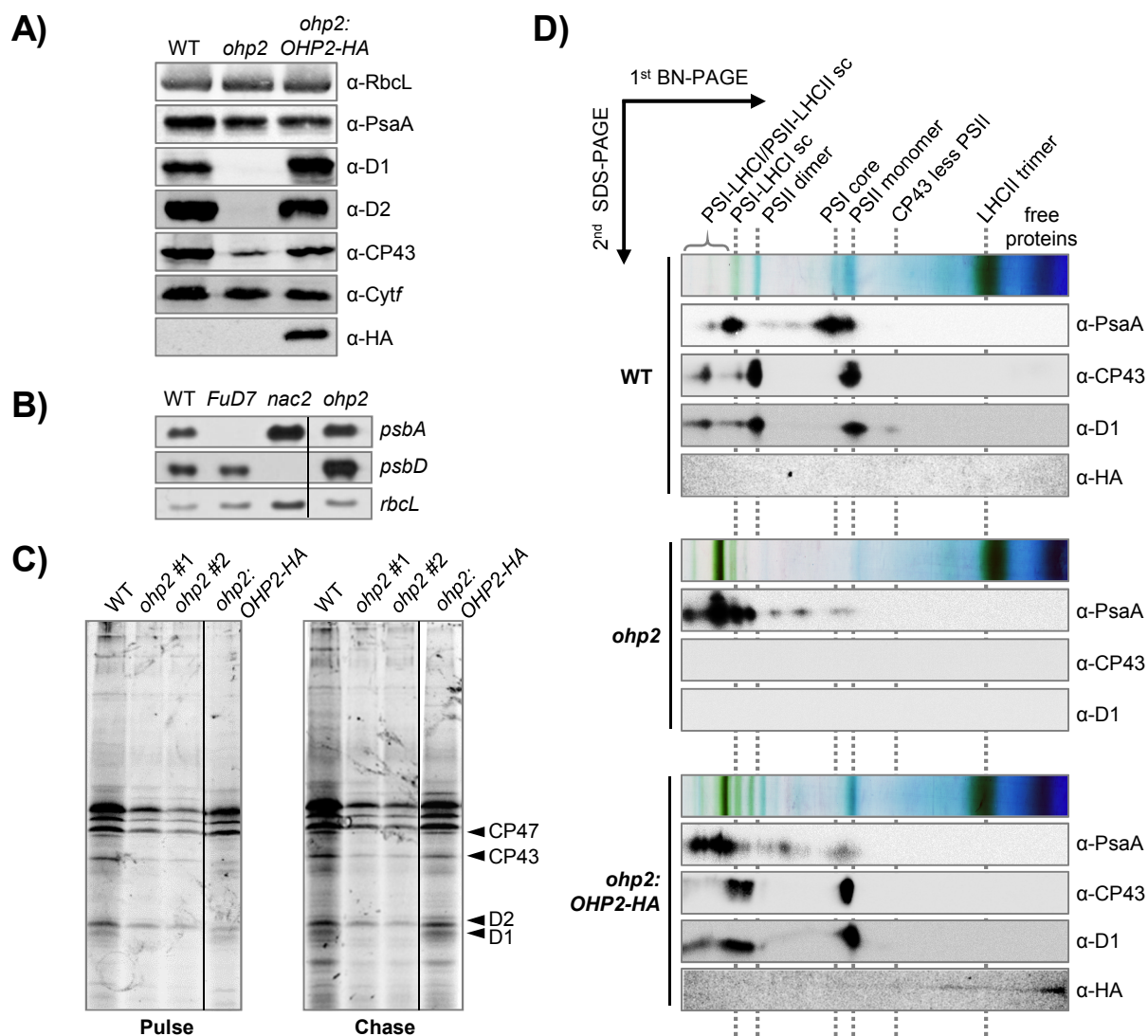


Figure 3. Drastically diminished D1 protein accumulation and synthesis in the *ohp2* mutant. The following strains were subjected to analysis: Jex4 (WT), *ohp2* and the complemented strain *ohp2:OHP2-HA* clone #53 (*ohp2:OHP2-HA*). **A)** Accumulation of photosynthesis related chloroplast proteins. 30 µg of total proteins from indicated strains were separated by 12% (α-D1, α-PsaA, α-Cytf, α-CP43, α-D2) or 15% (α-HA, α-RbcL) denaturing polyacrylamide gels and analyzed by the antibodies indicated. **B)** Accumulation of photosynthesis related chloroplast transcripts. 3 µg of total cellular RNA from indicated strains were fractionated by denaturing agarose gel electrophoresis and blotted onto a nylon membrane. Membranes were hybridized with probes specific for *psbA* and *psbD*. For loading control, the same blot was hybridized with a probe specific for *rbcL* transcripts. *nac2* and *FuD7* mutants were employed as negative controls for *psbD* or *psbA* mRNA accumulation, respectively. *ohp2* was run on the same gel but not in adjacent lanes as indicated by a vertical black line. **C)** Synthesis of PSII subunits. ¹⁴C labelling of chloroplast-encoded proteins was performed as described previously in Spaniol et al. (2021). Autoradiogram of cells pulsed for 5 min with ¹⁴C-acetate in the presence of cycloheximide (left), then chased for 45 min after washing and chloramphenicol addition. For *ohp2*, two independently grown cultures (#1, #2) were analyzed. The complemented strain was run on the same gel and exposed in the same conditions, but in non-adjacent lanes as indicated by a vertical black line. **D)** 2D BN-PAGE analysis of photosynthetic protein complexes in indicated strains. After solubilization of membranes with 1.5% (w/v) dodecyl-b-D-maltopyranoside, thylakoid proteins were separated by 5 to 12 % BN gels in the first dimension and 12% SDS-gels in the second dimension. Photosynthetic complexes were detected using the indicated antibodies. The positions of major PSI and PSII complexes are designated. sc: supercomplex

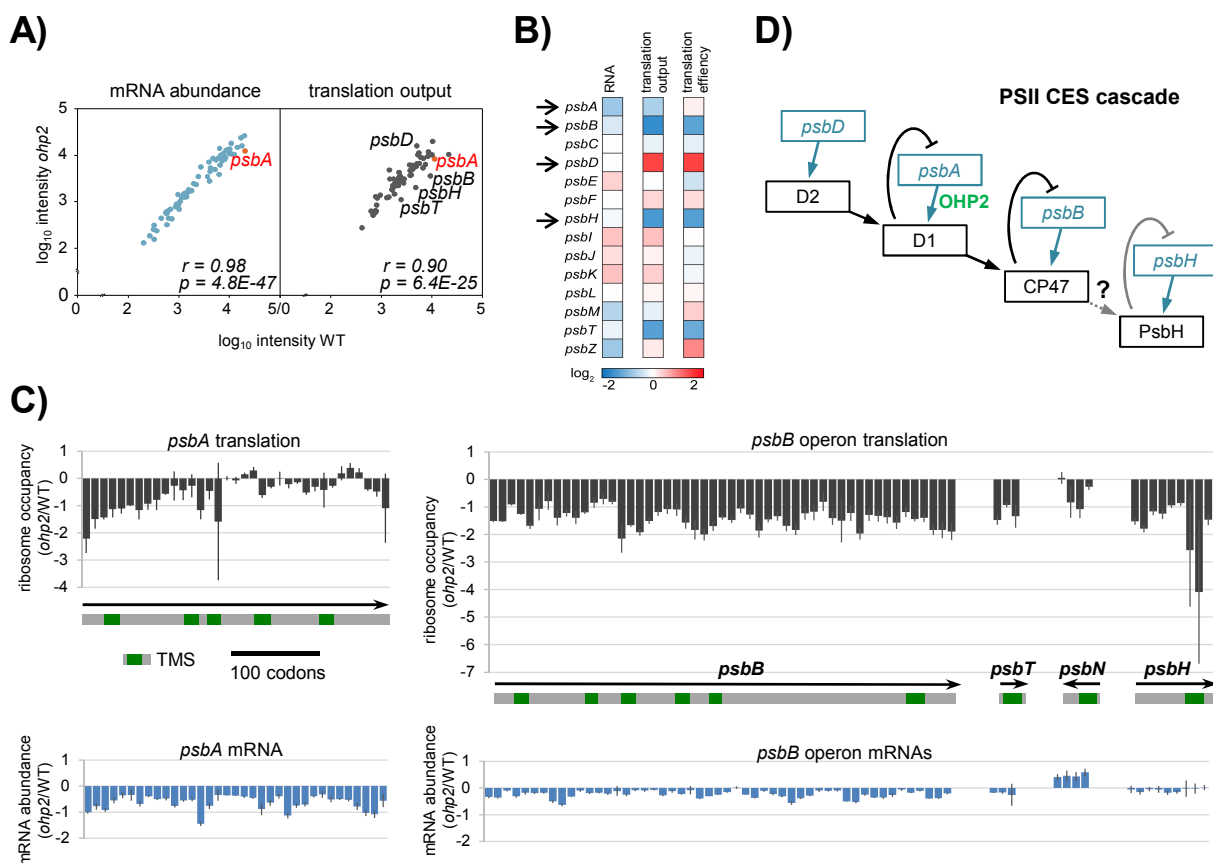


Figure 4. Targeted ribosome profiling of chloroplast translation reveals protein synthesis defects in the *ohp2* mutant. Ribosome profiling and transcript analysis of WT and *ohp2* mutant grown mixotrophically under $30 \mu\text{E}/\text{m}^2/\text{s}$. **A)** The average mRNA (blue) and ribosome FP (dark grey) abundances were calculated from three independent biological replicates and plotted in \log_{10} scale for *ohp2* mutant versus WT, respectively. mRNAs encoding PSII subunits, which display altered translation in the mutant are highlighted. *Pearsons's r*-value and *p*-value are given in *nEm* non-superscript format for $n \cdot 10m$. **B)** The relative average transcript abundances (RNA), translation output and translation efficiency were calculated for each chloroplast reading frame in both *Chlamydomonas* strains, normalized to overall signal intensities, and plotted as heat map (*ohp2* versus WT) in \log_2 scale. Increased RNA accumulation, translation output or translation efficiency in the mutant is shown in red, reduced levels are shown in blue (see scale bar). PSII subunits that are further discussed are highlighted with an arrow. **C)** For the Open Reading Frames (ORFs) of *psbA* (introns not shown) and the *psbB* operon normalized ribosome FP intensities were plotted as mean \log_2 ratios between *ohp2* mutant and WT. Error bars denote differences between three independent biological replicates. Grey bars below the panels indicate respective ORFs with trans-membrane segments (TMS in green). Related to Supplemental Figures S6, S7 and Supplemental Dataset 1. **D)** CES cascade of PSII. When newly synthesized CES polypeptides, like D1 and CP47, cannot assemble, they repress the translation initiation of their encoding mRNA as described before by Minai and coworkers (2006). Reduced translation of *psbH* may indicate that it represents a further component of the CES cascade.

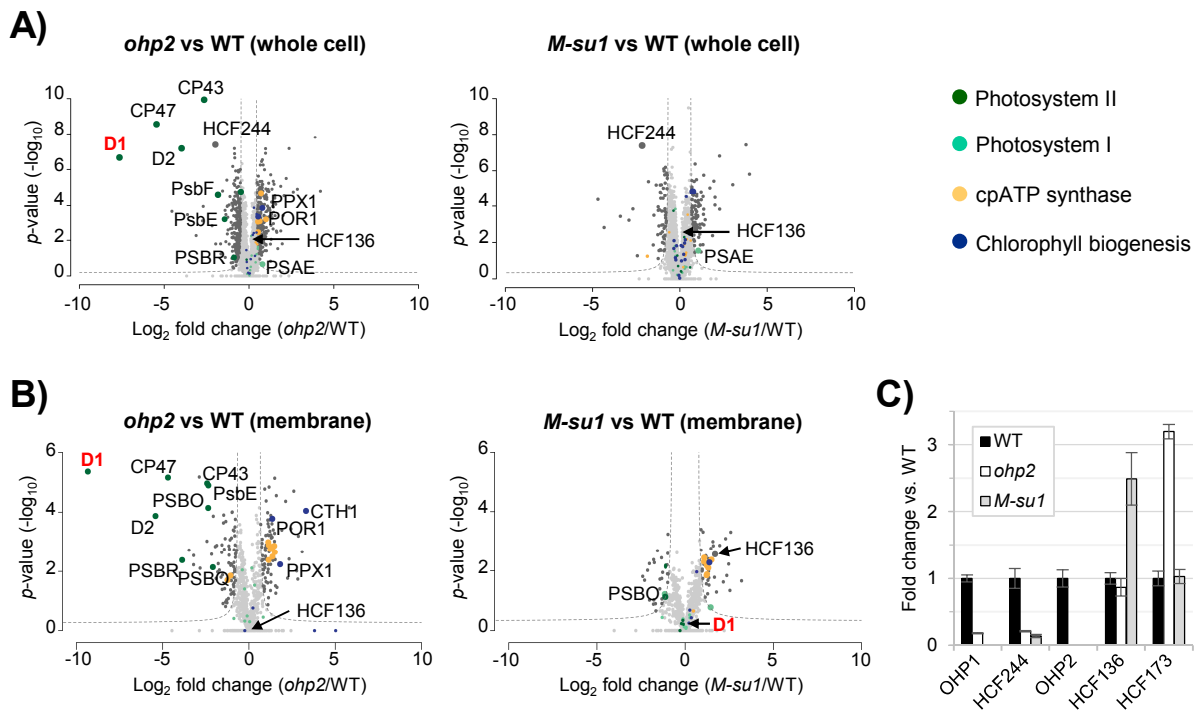


Figure 5. Altered proteome composition in the *ohp2* mutant and the suppressor strain. Volcano plots representing the relative proteome changes of whole cell lysates (**A**) of *ohp2* mutant versus WT (left), suppressor line 1 versus WT (right) and thylakoid membrane proteins (**B**) as comparison between *ohp2* mutant versus WT (left) and suppressor line 1 versus WT (right). For B), proteins of the membrane fraction were enriched by crude fractionation. All experiments were performed in at least three independent biological replicates. Mean fold change of LFQ values (in \log_2) is plotted on the x-axis, p -values (in $-\log_{10}$) are plotted on the y-axis. Light grey dots represent proteins with no significant change, dark grey dots show proteins that are significantly different with $FDR < 0.05$ and $S_0 = 1$. Proteins of PSI, PSII, the chloroplast ATP synthase, and of proteins involved in Chl biogenesis are marked in color as depicted in the legend on the right. Large colored dots are significantly different. **C)** Abundance of selected proteins in membrane protein extracts as determined by targeted mass spectrometry in different strains as compared to WT. Error bars indicate standard deviation over three biological replicates. Missing values indicate instances where no peptides could be found or are present below baseline signal of app. 5% compared to WT as judging from dotp values and fragment coelution profiles.

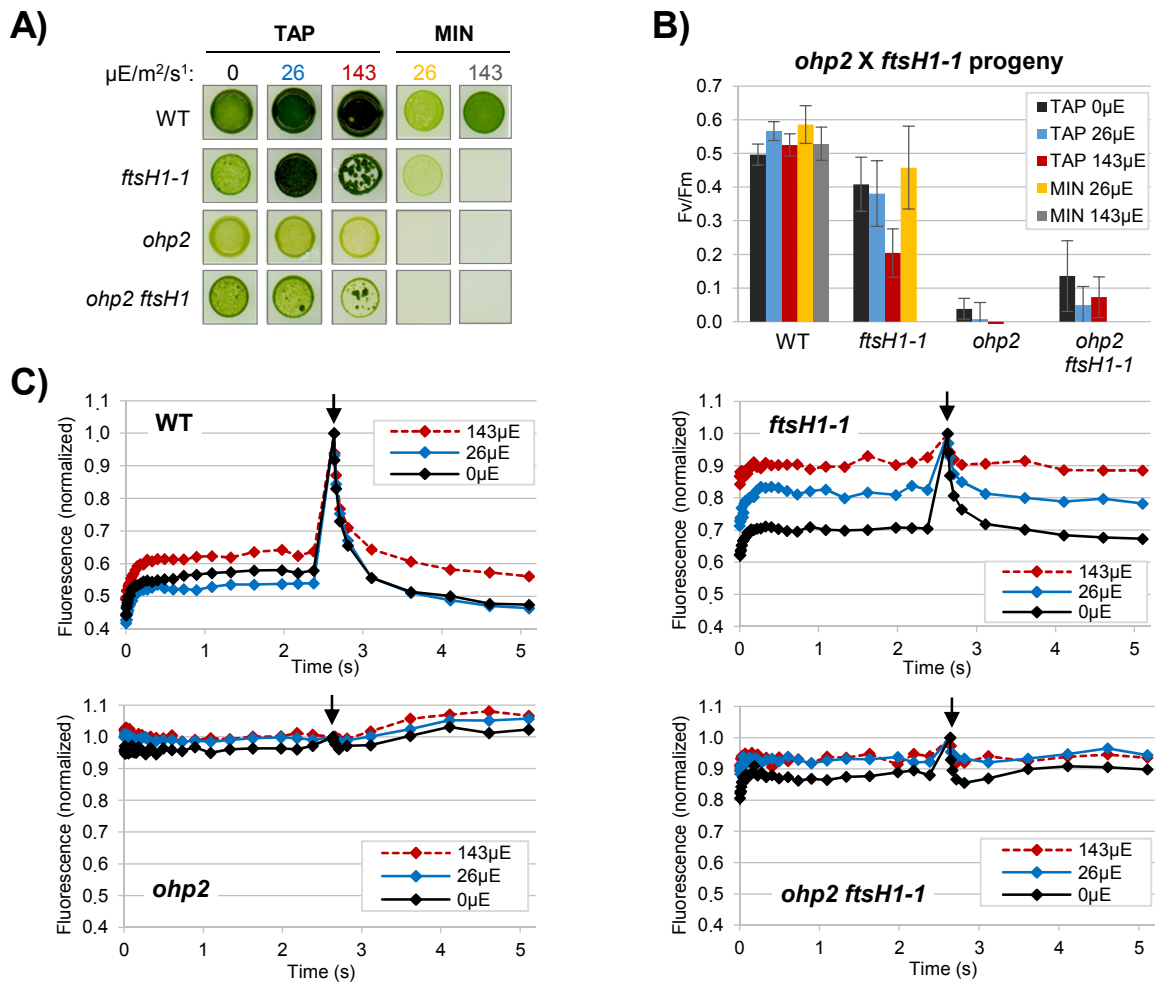


Figure 6. Mutation of the FtsH protease partially restores PSII activity but not photoautotrophy. **A)** Growth tests of the progeny of a cross *10.1a X ftsH1-1*. Cells were grown on TAP or MIN medium at the indicated light intensity. Spots shown are typical of the indicated genotypes. **B)** Fv/Fm values for the four genotypes, recorded from the plates in A). Values are average of 8, 7, 11 and 6 strains for the WT, *ftsH1*, *ohp2* and *ohp2 ftsH1* genotypes, respectively. Error bars represent S.D. **C)** Typical fluorescence induction curves for the four genotypes, recorded with the fluorescence camera on the TAP plates described in A). Fluorescence is normalized to the Fm value (arrow indicates saturating flash).

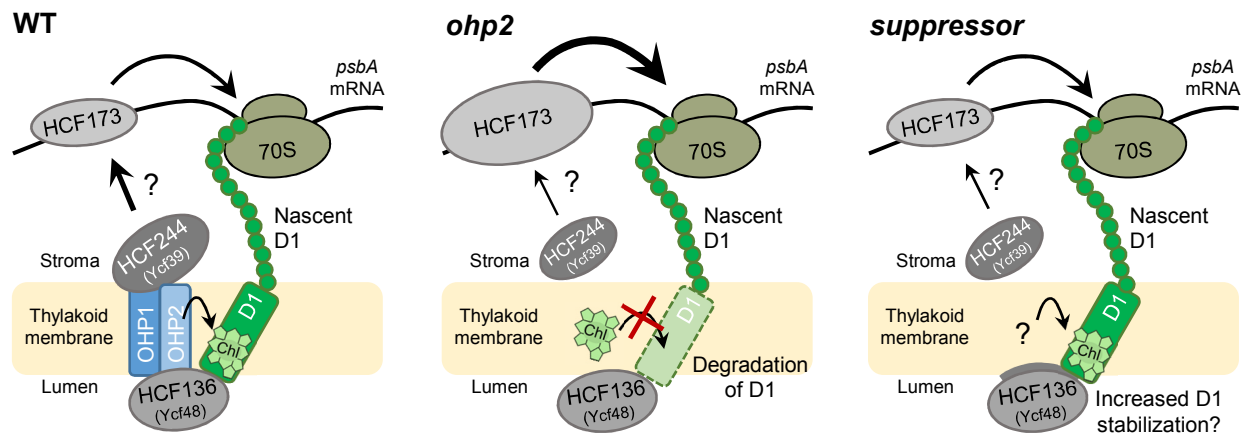


Figure 7. Schematic model for the role the OHC complex and associated proteins in D1 synthesis and first steps of PSII de novo assembly. In the WT (left panel), likely triggered by HCF244, HCF173 binds the 5'-UTR of *psbA* mRNA to promote translation initiation. pD1 is co-translationally inserted into the thylakoid membrane. Membrane associated luminal HCF136 stabilizes pD1 and is involved in RC assembly. The OHC is required for early PSII assembly steps and proposed to insert Chl into pD1 proteins. Recently reported negative autoregulatory circuits of *psbA* translation initiation involving the OHC are not displayed here (Chotewutmontri and Barkan, 2020; Chotewutmontri et al., 2020). In *ohp2* (middle panel) and suppressor strains (right panel) residual levels of HCF244 may promote *psbA* translation via interaction with HCF173. Ongoing *psbA* translation may be further supported by overaccumulation of HCF173. However, in the *ohp2* mutant synthesized D1 is rapidly degraded and does not accumulate in the absence of the OHC complex. In the suppressor strains, stabilization of nascent D1 may be accomplished by increased membrane association of HCF136 or other mechanisms to allow assembly of early PSII intermediates. HCF173, HCF136, and HCF244 protein amounts detected by proteomics are indicated by differently sized ovals. Names of cyanobacterial homologs are given in brackets.

Parsed Citations

- Andersson, U., Heddad, M., and Adamska, I. (2003). Light stress-induced one-helix protein of the chlorophyll a/b-binding family associated with photosystem I. *Plant Physiol*, 132: 811-820. <https://doi.org/10.1104/pp.102.019281>
Google Scholar: [Author Only](#) [Title Only](#) [Author and Title](#)
- Avramov, A.P., Hwang, H.J., and Burnap, R.L. (2020). The role of Ca²⁺ and protein scaffolding in the formation of nature's water oxidizing complex. *Proc Natl Acad Sci USA*, 117: 28036-28045. <https://doi.org/10.1073/pnas.2011315117>
Google Scholar: [Author Only](#) [Title Only](#) [Author and Title](#)
- Beck, J., Lohscheider, J.N., Albert, S., Andersson, U., Mendgen, K.W., Rojas-Stütz, M.C., Adamska, I., and Funck, D. (2017). Small One-Helix Proteins are essential for photosynthesis in Arabidopsis. *Front Plant Sci*, 8. <https://doi.org/10.3389/fpls.2017.00007>
Google Scholar: [Author Only](#) [Title Only](#) [Author and Title](#)
- Bečková, M., Yu, J., Krynická, V., Kozlo, A., Shao, S., Koník, P., Komenda, J., Murray, J.W., and Nixon, P.J. (2017). Structure of Psb29/Thf1 and its association with the FtsH protease complex involved in photosystem II repair in cyanobacteria. *Philos Trans R Soc Lond B Biol Sci*, 372: 20160394. <https://doi.org/10.1098/rstb.2016.0394>
Google Scholar: [Author Only](#) [Title Only](#) [Author and Title](#)
- Bennoun, P., Spierer-Herz, M., Erickson, J., Girard-Bascou, J., Pierre, Y., Delosme, M., and Rochaix, J.D. (1986). Characterization of photosystem II mutants of *Chlamydomonas reinhardtii* lacking the psbA gene. *Plant Mol Biol*, 6: 151-160. <https://doi.org/10.1007/bf00021484>
Google Scholar: [Author Only](#) [Title Only](#) [Author and Title](#)
- Boudreau, E., Nickelsen, J., Lemaire, S.D., Ossenbühl, F., and Rochaix, J.-D. (2000). The Nac2 gene of *Chlamydomonas* encodes a chloroplast TPR-like protein involved in psbD mRNA stability. *EMBO J*, 19: 3366-3376. <https://doi.org/10.1093/emboj/19.13.3366>
Google Scholar: [Author Only](#) [Title Only](#) [Author and Title](#)
- Bradford, M.M. (1976). A rapid and sensitive method for the quantitation of microgram quantities of protein utilizing the principle of protein-dye binding. *Anal Biochem*, 72: 248-254. <https://doi.org/10.1006/abio.1976.9999>
Google Scholar: [Author Only](#) [Title Only](#) [Author and Title](#)
- Cavaiuolo, M., Kuras, R., Wollman, F.A., Choquet, Y., and Vallon, O. (2017). Small RNA profiling in *Chlamydomonas*: insights into chloroplast RNA metabolism. *Nucleic Acids Res*, 45: 10783-10799. <https://doi.org/10.1093/nar/gkx668>
Google Scholar: [Author Only](#) [Title Only](#) [Author and Title](#)
- Cecchin, M., Jeong, J., Son, W., Kim, M., Park, S., Zuliani, L., Cazzaniga, S., Pompa, A., Young Kang, C., Bae, S., Ballottari, M., and Jin, E. (2021). LPA2 protein is involved in photosystem II assembly in *Chlamydomonas reinhardtii*. *Plant J*, 107: 1648-1662. <https://doi.org/10.1111/tpj.15405>
Google Scholar: [Author Only](#) [Title Only](#) [Author and Title](#)
- Chidgey, J.W., Linhartová, M., Komenda, J., Jackson, P.J., Dickman, M.J., Canniffe, D.P., Koník, P., Pilný, J., Hunter, C.N., and Sobotka, R. (2014). A cyanobacterial chlorophyll synthase-HliD complex associates with the Ycf39 protein and the YidC/Alb3 insertase. *Plant Cell*, 26: 1267-1279. <https://doi.org/10.1105/tpc.114.124495>
Google Scholar: [Author Only](#) [Title Only](#) [Author and Title](#)
- Choquet, Y., and Wollman, F.-A. (2009). The CES Process. In E. H. Harris, D. B. Stern, & G. B. Witman (Eds.), *The Chlamydomonas Sourcebook* (Second Edition) (pp. 1027-1063). Academic Press. <https://doi.org/10.1016/B978-0-12-370873-1.00037-X>
Google Scholar: [Author Only](#) [Title Only](#) [Author and Title](#)
- Chotewutmontri, P., and Barkan, A. (2018). Multilevel effects of light on ribosome dynamics in chloroplasts program genome-wide and psbA-specific changes in translation. *PLoS Genet*, 14: e1007555. <https://doi.org/10.1371/journal.pgen.1007555>
Google Scholar: [Author Only](#) [Title Only](#) [Author and Title](#)
- Chotewutmontri, P., and Barkan, A. (2020). Light-induced psbA translation in plants is triggered by photosystem II damage via an assembly-linked autoregulatory circuit. *Proc Natl Acad Sci USA*, 117: 21775-21784. <https://doi.org/10.1073/pnas.2007833117>
Google Scholar: [Author Only](#) [Title Only](#) [Author and Title](#)
- Chotewutmontri, P., Williams-Carrier, R., and Barkan, A. (2020). Exploring the link between photosystem II assembly and translation of the chloroplast psbA mRNA. *Plants*, 9: 152. <https://doi.org/10.3390/plants9020152>
Google Scholar: [Author Only](#) [Title Only](#) [Author and Title](#)
- Cox, J., Hein, M.Y., Luber, C.A., Paron, I., Nagaraj, N., and Mann, M. (2014). Accurate proteome-wide label-free quantification by delayed normalization and maximal peptide ratio extraction, termed MaxLFQ. *Mol Cell Proteomics*, 13: 2513-2526. <https://doi.org/10.1074/mcp.M113.031591>
Google Scholar: [Author Only](#) [Title Only](#) [Author and Title](#)
- Cox, J., and Mann, M. (2008). MaxQuant enables high peptide identification rates, individualized p.p.b.-range mass accuracies and proteome-wide protein quantification. *Nat Biotechnol*, 26: 1367-1372. <https://doi.org/10.1038/nbt.1511>
Google Scholar: [Author Only](#) [Title Only](#) [Author and Title](#)

Day, A., Schirmer-Rahire, M., Kuchka, M.R., Mayfield, S.P., and Rochaix, J.D. (1988). A transposon with an unusual arrangement of long terminal repeats in the green alga *Chlamydomonas reinhardtii*. *EMBO J*, 7: 1917-1927. <https://doi.org/10.1002/j.1460-2075.1988.tb03029.x>

Google Scholar: [Author Only](#) [Title Only](#) [Author and Title](#)

de Vitry, C., Olive, J., Drapier, D., Recouvreur, M., and Wollman, F.A. (1989). Posttranslational events leading to the assembly of photosystem II protein complex: a study using photosynthesis mutants from *Chlamydomonas reinhardtii*. *J Cell Biol*, 109: 991-1006. <https://doi.org/10.1083/jcb.109.3.991>

Google Scholar: [Author Only](#) [Title Only](#) [Author and Title](#)

Emanuelsson, O., Nielsen, H., Brunak, S., and von Heijne, G. (2000). Predicting subcellular localization of proteins based on their N-terminal amino acid sequence. *J Mol Biol*, 300: 1005-1016. <https://doi.org/10.1006/jmbi.2000.3903>

Google Scholar: [Author Only](#) [Title Only](#) [Author and Title](#)

Engelken, J., Brinkmann, H., and Adamska, I. (2010). Taxonomic distribution and origins of the extended LHC (light-harvesting complex) antenna protein superfamily. *BMC Evol Biol*, 10: 233. <https://doi.org/10.1186/1471-2148-10-233>

Google Scholar: [Author Only](#) [Title Only](#) [Author and Title](#)

Falciatore, A., Merendino, L., Barneche, F., Ceol, M., Meskauskiene, R., Apel, K., and Rochaix, J.-D. (2005). The FLP proteins act as regulators of chlorophyll synthesis in response to light and plastid signals in *Chlamydomonas*. *Genes Dev*, 19: 176-187. <https://doi.org/10.1101/gad.321305>

Google Scholar: [Author Only](#) [Title Only](#) [Author and Title](#)

Ferris, P.J., Armbrust, E.V., and Goodenough, U.W. (2002). Genetic structure of the mating-type locus of *Chlamydomonas reinhardtii*. *Genetics*, 160: 181-200. <https://doi.org/10.1093/genetics/160.1.181>

Google Scholar: [Author Only](#) [Title Only](#) [Author and Title](#)

Friedt, R., Herdean, A., Blaby-Haas, C.E., Mamedov, F., Merchant, S.S., Last, R.L., and Lundin, B. (2015). PHOTOSYSTEM II PROTEIN33, a protein conserved in the plastid lineage, is associated with the chloroplast thylakoid membrane and provides stability to photosystem II supercomplexes in *Arabidopsis*. *Plant Physiol*, 167: 481-492. <https://doi.org/10.1104/pp.114.253336>

Google Scholar: [Author Only](#) [Title Only](#) [Author and Title](#)

Gao, J., Wang, H., Yuan, Q., and Feng, Y. (2018). Structure and function of the photosystem supercomplexes. *Front Plant Sci*, 9. <https://doi.org/10.3389/fpls.2018.00357>

Google Scholar: [Author Only](#) [Title Only](#) [Author and Title](#)

Gessulat, S., Schmidt, T., Zolg, D.P., Samaras, P., Schnatbaum, K., Zerweck, J., Knaute, T., Rechenberger, J., Delanghe, B., Huhmer, A., Reimer, U., Ehrlich, H.-C., Aiche, S., Kuster, B., and Wilhelm, M. (2019). Prosit: proteome-wide prediction of peptide tandem mass spectra by deep learning. *Nat Meth*, 16: 509-518. <https://doi.org/10.1038/s41592-019-0426-7>

Google Scholar: [Author Only](#) [Title Only](#) [Author and Title](#)

Girard-Bascou, J., Pierre, Y., and Drapier, D. (1992). A nuclear mutation affects the synthesis of the chloroplast psbA gene production *Chlamydomonas reinhardtii*. *Curr Genet*, 22: 47-52. <https://doi.org/10.1007/BF00351741>

Google Scholar: [Author Only](#) [Title Only](#) [Author and Title](#)

Hammel, A., Zimmer, D., Sommer, F., Mühlhaus, T., and Schroda, M. (2018). Absolute quantification of major photosynthetic protein complexes in *Chlamydomonas reinhardtii* using quantification concatamers (QconCATs). *Front Plant Sci*, 9. <https://doi.org/10.3389/fpls.2018.01265>

Google Scholar: [Author Only](#) [Title Only](#) [Author and Title](#)

Harris, E.H. (2009). The *Chlamydomonas* Sourcebook: Introduction to *Chlamydomonas* and Its Laboratory Use. In E. H. Harris, D. B. Stern, & G. B. Witman (Eds.), (Second Edition ed., Vol. 1). Academic press.

Google Scholar: [Author Only](#) [Title Only](#) [Author and Title](#)

Heddad, M., Engelken, J., and Adamska, I. (2012). Light stress proteins in viruses, cyanobacteria and photosynthetic Eukaryota. In J. J. Eaton-Rye, B. C. Tripathy, & T. D. Sharkey (Eds.), *Photosynthesis: Plastid Biology, Energy Conversion and Carbon Assimilation* (Vol. 34, pp. 299-318). Springer.

Google Scholar: [Author Only](#) [Title Only](#) [Author and Title](#)

Heinz, S., Liauw, P., Nickelsen, J., and Nowaczyk, M. (2016). Analysis of photosystem II biogenesis in cyanobacteria. *Biochimica et Biophysica Acta (BBA) - Bioenergetics*, 1857: 274-287. <https://doi.org/10.1016/j.bbabi.2015.11.007>

Google Scholar: [Author Only](#) [Title Only](#) [Author and Title](#)

Hey, D., and Grimm, B. (2018). ONE-HELIX PROTEIN2 (OHP2) is required for the stability of OHP1 and assembly factor HCF244 and is functionally linked to PSII biogenesis. *Plant Physiol*, 177: 1453-1472. <https://doi.org/10.1104/pp.18.00540>

Google Scholar: [Author Only](#) [Title Only](#) [Author and Title](#)

Hey, D., and Grimm, B. (2020). ONE-HELIX PROTEIN1 and 2 form heterodimers to bind chlorophyll in photosystem II biogenesis. *Plant Physiol*, 183: 179-193. <https://doi.org/10.1104/pp.19.01304>

Google Scholar: [Author Only](#) [Title Only](#) [Author and Title](#)

- Hofmann, K.P., and Stoffel, W. (1993). TMBASE-a database of membrane spanning protein segments. *Biol Chem Hoppe Seyler*, 374: 166.
Google Scholar: [Author Only](#) [Title Only](#) [Author and Title](#)
- Houille-Vernes, L., Rappaport, F., Wollman, F.-A., Alric, J., and Johnson, X. (2011). Plastid terminal oxidase 2 (PTOX2) is the major oxidase involved in chlororespiration in *Chlamydomonas*. *Proc Natl Acad Sci USA*, 108: 20820-20825.
<https://doi.org/10.1073/pnas.1110518109>
Google Scholar: [Author Only](#) [Title Only](#) [Author and Title](#)
- Hu, F., Zhu, Y., Wu, W., Xie, Y., and Huang, J. (2015). Leaf variegation of Thylakoid Formation1 is suppressed by mutations of specific σ -factors in *Arabidopsis*. *Plant Physiol*, 168: 1066-1075. <https://doi.org/10.1104/pp.15.00549>
Google Scholar: [Author Only](#) [Title Only](#) [Author and Title](#)
- Huang, G., Xiao, Y., Pi, X., Zhao, L., Zhu, Q., Wang, W., Kuang, T., Han, G., Sui, S.-F., and Shen, J.-R. (2021). Structural insights into a dimeric Psb27-photosystem II complex from a cyanobacterium *Thermosynechococcus vulcanus*. *Proc Natl Acad Sci USA*, 118: e2018053118. <https://doi.org/10.1073/pnas.2018053118>
Google Scholar: [Author Only](#) [Title Only](#) [Author and Title](#)
- Huang, W., Chen, Q., Zhu, Y., Hu, F., Zhang, L., Ma, Z., He, Z., and Huang, J. (2013). *Arabidopsis* Thylakoid Formation 1 is a critical regulator for dynamics of PSII-LHCII complexes in leaf senescence and excess light. *Mol Plant*, 6: 1673-1691.
<https://doi.org/10.1093/mp/sst069>
Google Scholar: [Author Only](#) [Title Only](#) [Author and Title](#)
- Jalal, A., Schwarz, C., Schmitz-Linneweber, C., Vallon, O., Nickelsen, J., and Bohne, A.-V. (2015). A small multifunctional pentatricopeptide repeat protein in the chloroplast of *Chlamydomonas reinhardtii*. *Mol Plant*, 8: 412-426.
<https://doi.org/10.1016/j.molp.2014.11.019>
Google Scholar: [Author Only](#) [Title Only](#) [Author and Title](#)
- Kato, Y., and Sakamoto, W. (2009). Protein quality control in chloroplasts: A current model of D1 protein degradation in the photosystem II repair cycle. *J Biochem*, 146: 463-469. <https://doi.org/10.1093/jb/mvp073>
Google Scholar: [Author Only](#) [Title Only](#) [Author and Title](#)
- Kim, J., Eichacker, L.A., Rudiger, W., and Mullet, J.E. (1994a). Chlorophyll regulates accumulation of the plastid-encoded chlorophyll proteins P700 and D1 by increasing apoprotein stability. *Plant Physiol*, 104: 907-916.
<https://doi.org/10.1104/pp.104.3.907>
Google Scholar: [Author Only](#) [Title Only](#) [Author and Title](#)
- Kim, J., Klein, P.G., and Mullet, J.E. (1991). Ribosomes pause at specific sites during synthesis of membrane-bound chloroplast reaction center protein D1. *J Biol Chem*, 266: 14931-14938. [https://doi.org/10.1016/S0021-9258\(18\)98567-4](https://doi.org/10.1016/S0021-9258(18)98567-4)
Google Scholar: [Author Only](#) [Title Only](#) [Author and Title](#)
- Kim, J., Klein, P.G., and Mullet, J.E. (1994b). Synthesis and turnover of photosystem II reaction center protein D1. Ribosome pausing increases during chloroplast development. *J Biol Chem*, 269: 17918-17923. [https://doi.org/10.1016/S0021-9258\(17\)32397-9](https://doi.org/10.1016/S0021-9258(17)32397-9)
Google Scholar: [Author Only](#) [Title Only](#) [Author and Title](#)
- Kindle, K.L. (1990). High-frequency nuclear transformation of *Chlamydomonas reinhardtii*. *Proc Natl Acad Sci USA*, 87: 1228-1232.
<https://doi.org/10.1073/pnas.87.3.1228>
Google Scholar: [Author Only](#) [Title Only](#) [Author and Title](#)
- Knoppová, J., Sobotka, R., Tichý, M., Yu, J., Konik, P., Halada, P., Nixon, P.J., and Komenda, J. (2014). Discovery of a chlorophyll binding protein complex involved in the early steps of photosystem II assembly in *Synechocystis*. *Plant Cell*, 26: 1200-1212.
<https://doi.org/10.1105/tpc.114.123919>
Google Scholar: [Author Only](#) [Title Only](#) [Author and Title](#)
- Komenda, J., Nickelsen, J., Tichy, M., Prásl, O., Eichacker, L.A., and Nixon, P.J. (2008). The cyanobacterial homologue of HCF136/YCF48 is a component of an early photosystem II assembly complex and is important for both the efficient assembly and repair of photosystem II in *Synechocystis* sp. PCC 6803. *J Biol Chem*, 283 No. 33: 22390-22399.
<https://doi.org/10.1074/jbc.M801917200>
Google Scholar: [Author Only](#) [Title Only](#) [Author and Title](#)
- Komenda, J., and Sobotka, R. (2016). Cyanobacterial high-light-inducible proteins - Protectors of chlorophyll-protein synthesis and assembly. *Biochimica et Biophysica Acta (BBA) - Bioenergetics*, 1857: 288-295. <https://doi.org/10.1016/j.bbabi.2015.08.011>
Google Scholar: [Author Only](#) [Title Only](#) [Author and Title](#)
- Komenda, J., Tichy, M., and Eichacker, L.A. (2005). The PsbH protein is associated with the inner antenna CP47 and facilitates D1 processing and incorporation into PSII in the cyanobacterium *Synechocystis* PCC 6803. *Plant Cell Physiol*, 46: 1477-1483.
<https://doi.org/10.1093/pcp/pci159>
Google Scholar: [Author Only](#) [Title Only](#) [Author and Title](#)
- Kühlbrandt, W., Wang, D.N., and Fujiyoshi, Y. (1994). Atomic model of plant light-harvesting complex by electron crystallography.

Nature, 367: 614 - 621. <https://doi.org/10.1038/367614a0>

Google Scholar: [Author Only](#) [Title Only](#) [Author and Title](#)

Kuras, R., de Vitry, C., Choquet, Y., Girard-Bascou, J., Culler, D., Büschlen, S., Merchant, S., and Wollman, F.-A. (1997). Molecular genetic identification of a pathway for heme binding to cytochrome b 6. *J Biol Chem*, 272: 32427-32435.

<https://doi.org/10.1074/jbc.272.51.32427>

Google Scholar: [Author Only](#) [Title Only](#) [Author and Title](#)

Lefebvre-Legendre, L., Choquet, Y., Kuras, R., Loubéry, S., Douchi, D., and Goldschmidt-Clermont, M. (2015). A nucleus-encoded chloroplast protein regulated by iron availability governs expression of the photosystem I subunit PsaA in *Chlamydomonas reinhardtii*. *Plant Physiol*, 167: 1527-1540. <https://doi.org/10.1104/pp.114.253906>

Google Scholar: [Author Only](#) [Title Only](#) [Author and Title](#)

Li, Y., Liu, B., Zhang, J., Kong, F., Zhang, L., Meng, H., Li, W., Rochaix, J.-D., Li, D., and Peng, L. (2019). OHP1, OHP2, and HCF244 form a transient functional complex with the photosystem II reaction center. *Plant Physiol*, 179: 195-208.

<https://doi.org/10.1104/pp.18.01231>

Google Scholar: [Author Only](#) [Title Only](#) [Author and Title](#)

Link, S., Engelmann, K., Meierhoff, K., and Westhoff, P. (2012). The atypical short-chain dehydrogenases HCF173 and HCF244 are jointly involved in translational initiation of the *psbA* mRNA of *Arabidopsis*. *Plant Physiol*, 160: 2202-2218.

<https://doi.org/10.1104/pp.112.205104>

Google Scholar: [Author Only](#) [Title Only](#) [Author and Title](#)

Loiselay, C., Gumpel, N.J., Girard-Bascou, J., Watson, A.T., Purton, S., Wollman, F.-A., and Choquet, Y. (2008). Molecular identification and function of cis- and trans-acting determinants for *petA* transcript stability in *Chlamydomonas reinhardtii* chloroplasts. *Mol Cell Biol*, 28: 5529-5542. <https://doi.org/10.1128/mcb.02056-07>

Google Scholar: [Author Only](#) [Title Only](#) [Author and Title](#)

Loizeau, K., Qu, Y., Depp, S., Fiechter, V., Ruwe, H., Lefebvre-Legendre, L., Schmitz-Linneweber, C., and Goldschmidt-Clermont, M. (2014). Small RNAs reveal two target sites of the RNA-maturation factor Mbb1 in the chloroplast of *Chlamydomonas*. *Nucleic Acids Res*, 42: 3286-3297. <https://doi.org/10.1093/nar/gkt1272>

Google Scholar: [Author Only](#) [Title Only](#) [Author and Title](#)

Lu, Y. (2016). Identification and roles of photosystem II assembly, stability, and repair factors in *Arabidopsis*. *Front Plant Sci*, 7. <https://doi.org/10.3389/fpls.2016.00168>

Google Scholar: [Author Only](#) [Title Only](#) [Author and Title](#)

MacLean, B., Tomazela, D.M., Shulman, N., Chambers, M., Finney, G.L., Frewen, B., Kern, R., Tabb, D.L., Liebler, D.C., and MacCoss, M.J. (2010). Skyline: an open source document editor for creating and analyzing targeted proteomics experiments. *Bioinformatics (Oxford, England)*, 26: 966-968. <https://doi.org/10.1093/bioinformatics/btq054>

Google Scholar: [Author Only](#) [Title Only](#) [Author and Title](#)

Malnoë, A., Wang, F., Girard-Bascou, J., Wollman, F.-A., and de Vitry, C. (2014). Thylakoid FtsH protease contributes to photosystem II and cytochrome b6f remodeling in *Chlamydomonas reinhardtii* under stress conditions. *Plant Cell*, 26: 373-390. <https://doi.org/10.1105/tpc.113.120113>

Google Scholar: [Author Only](#) [Title Only](#) [Author and Title](#)

Malnoë, A., Wollman, F.-A., de Vitry, C., and Rappaport, F. (2011). Photosynthetic growth despite a broken Q-cycle. *Nat Commun*, 2: 301-301. <https://doi.org/10.1038/ncomms1299>

Google Scholar: [Author Only](#) [Title Only](#) [Author and Title](#)

Martins, L., Knuesting, J., Bariat, L., Dard, A., Freibert, S.A., Marchand, C.H., Young, D., Dung, N.H.T., Voth, W., Debures, A., Saez-Vasquez, J., Lemaire, S.D., Lill, R., Messens, J., Scheibe, R., Reichheld, J.P., and Riondet, C. (2020). Redox modification of the Iron-Sulfur Glutaredoxin GRXS17 activates holdase activity and protects plants from heat stress. *Plant Physiol*, 184: 676-692. <https://doi.org/10.1104/pp.20.00906>

Google Scholar: [Author Only](#) [Title Only](#) [Author and Title](#)

McDermott, J.J., Watkins, K.P., Williams-Carrier, R., and Barkan, A. (2019). Ribonucleoprotein capture by in vivo expression of a designer Pentatricopeptide Repeat Protein in *Arabidopsis*. *Plant Cell*, 31: 1723-1733. <https://doi.org/10.1105/tpc.19.00177>

Google Scholar: [Author Only](#) [Title Only](#) [Author and Title](#)

Meurer, J., Plucken, H., Kowallik, K.V., and Westhoff, P. (1998). A nuclear-encoded protein of prokaryotic origin is essential for the stability of photosystem II in *Arabidopsis thaliana*. *EMBO J*, 17: 5286-5297. <https://doi.org/10.1093/emboj/17.18.5286>

Google Scholar: [Author Only](#) [Title Only](#) [Author and Title](#)

Minai, L., Wostrikoff, K., Wollman, F.-A., and Choquet, Y. (2006). Chloroplast biogenesis of photosystem II cores involves a series of assembly-controlled steps that regulate translation. *Plant Cell*, 18: 159-175. <https://doi.org/10.1105/tpc.105.037705>

Google Scholar: [Author Only](#) [Title Only](#) [Author and Title](#)

Monod, C., Goldschmidt-Clermont, M., and Rochaix, J.D. (1992). Accumulation of chloroplast *psbB* RNA requires a nuclear factor

in *Chlamydomonas reinhardtii*. *Mol Gen Genet*, 231: 449-459. <https://doi.org/10.1007/BF00292715>

Google Scholar: [Author Only](#) [Title Only](#) [Author and Title](#)

Myouga, F., Takahashi, K., Tanaka, R., Nagata, N., Kiss, A.Z., Funk, C., Nomura, Y., Nakagami, H., Jansson, S., and Shinozaki, K. (2018). Stable accumulation of photosystem II requires ONE-HELIX PROTEIN1 (OHP1) of the light harvesting-like family. *Plant Physiol*, 176: 2277-2291. <https://doi.org/10.1104/pp.17.01782>

Google Scholar: [Author Only](#) [Title Only](#) [Author and Title](#)

Neupert, J., Karcher, D., and Bock, R. (2009). Generation of *Chlamydomonas* strains that efficiently express nuclear transgenes. *Plant J*, 57: 1140-1150. <https://doi.org/10.1111/j.1365-313X.2008.03746.x>

Google Scholar: [Author Only](#) [Title Only](#) [Author and Title](#)

Nicholas, K.B., Nicholas, H.B., and Deerfield, D.W. (1997). GeneDoc: analysis and visualization of genetic variation. *EMBNET NEWS*, 4: 14. [citeulike-article-id:3198041](https://doi.org/10.1101/1365-313X.2008.03746.x)

Google Scholar: [Author Only](#) [Title Only](#) [Author and Title](#)

Nickelsen, J., and Rengstl, B. (2013). Photosystem II assembly: From cyanobacteria to plants. *Ann Rev Plant Biol*, 64: 609-635. <https://doi.org/10.1146/annurev-arplant-050312-120124>

Google Scholar: [Author Only](#) [Title Only](#) [Author and Title](#)

Nielsen, H., Engelbrecht, J., Brunak, S., and von Heijne, G. (1997). Identification of prokaryotic and eukaryotic signal peptides and prediction of their cleavage sites. *Protein Eng*, 10: 1-6. <https://doi.org/10.1093/protein/10.1.1>

Google Scholar: [Author Only](#) [Title Only](#) [Author and Title](#)

Nilsson, A.K., Pěncík, A., Johansson, O.N., Bånkestad, D., Fristedt, R., Suorsa, M., Trotta, A., Novák, O., Mamedov, F., Aro, E.-M., and Burmeister, B.L. (2020). PSB33 protein sustains photosystem II in plant chloroplasts under UV-A light. *J Exp Bot*, 71: 7210-7223. <https://doi.org/10.1093/jxb/eraa427>

Google Scholar: [Author Only](#) [Title Only](#) [Author and Title](#)

Nixon, P.J., Michoux, F., Yu, J., Boehm, M., and Komenda, J. (2010). Recent advances in understanding the assembly and repair of photosystem II. *Ann Bot*, 106: 1-16. <https://doi.org/10.1093/aob/mcq059>

Google Scholar: [Author Only](#) [Title Only](#) [Author and Title](#)

O'Connor, H.E., Ruffle, S.V., Cain, A.J., Deak, Z., Vass, I., Nugent, J.H.A., and Purton, S. (1998). The 9-kDa phosphoprotein of photosystem II: Generation and characterisation of *Chlamydomonas* mutants lacking PSII-H and a site-directed mutant lacking the phosphorylation site. *Biochimica et Biophysica Acta (BBA) - Bioenergetics*, 1364: 63-72. [https://doi.org/10.1016/S0005-2728\(98\)00013-9](https://doi.org/10.1016/S0005-2728(98)00013-9)

Google Scholar: [Author Only](#) [Title Only](#) [Author and Title](#)

Pan, X., Ma, J., Su, X., Cao, P., Chang, W., Liu, Z., Zhang, X., and Li, M. (2018). Structure of the maize photosystem I supercomplex with light-harvesting complexes I and II. *Science*, 360: 1109-1113. <https://doi.org/10.1126/science.aat1156>

Google Scholar: [Author Only](#) [Title Only](#) [Author and Title](#)

Pérez-Pérez, M.E., Mauriès, A., Maes, A., Tourasse, N.J., Hamon, M., Lemaire, S.D., and Marchand, C.H. (2017). The deep thioredoxome in *Chlamydomonas reinhardtii*: New insights into redox regulation. *Mol Plant*, 10: 1107-1125. <https://doi.org/10.1016/j.molp.2017.07.009>

Google Scholar: [Author Only](#) [Title Only](#) [Author and Title](#)

Perez-Riverol, Y., Bai, J., Bandla, C., García-Seisdedos, D., Hewapathirana, S., Kamatchinathan, S., Kundu, Deepti J., Prakash, A., Frericks-Zipper, A., Eisenacher, M., Walzer, M., Wang, S., Brazma, A., and Vizcaíno, Juan A. (2021). The PRIDE database resources in 2022: a hub for mass spectrometry-based proteomics evidences. *Nucleic Acids Res*, 50: D543-D552. <https://doi.org/10.1093/nar/gkab1038>

Google Scholar: [Author Only](#) [Title Only](#) [Author and Title](#)

Pino, L.K., Searle, B.C., Bollinger, J.G., Nunn, B., MacLean, B., and MacCoss, M.J. (2020). The Skyline ecosystem: Informatics for quantitative mass spectrometry proteomics. *Mass Spectrom Rev*, 39: 229-244. <https://doi.org/10.1002/mas.21540>

Google Scholar: [Author Only](#) [Title Only](#) [Author and Title](#)

Plöchinger, M., Schwenkert, S., von Sydow, L., Schröder, W.P., and Meurer, J. (2016). Functional update of the auxiliary proteins PsbW, PsbY, HCF136, PsbN, TerC and ALB3 in maintenance and assembly of PSII. *Front Plant Sci*, 7. <https://doi.org/10.3389/fpls.2016.00423>

Google Scholar: [Author Only](#) [Title Only](#) [Author and Title](#)

Plücken, H., Müller, B., Grohmann, D., Westhoff, P., and Eichacker, L.A. (2002). The HCF136 protein is essential for assembly of the photosystem II reaction center in *Arabidopsis thaliana*. *FEBS Lett*, 532: 85-90. [https://doi.org/10.1016/s0014-5793\(02\)03634-7](https://doi.org/10.1016/s0014-5793(02)03634-7)

Google Scholar: [Author Only](#) [Title Only](#) [Author and Title](#)

Psencik, J., Hey, D., Grimm, B., and Lokstein, H. (2020). Photoprotection of photosynthetic pigments in plant One-Helix Protein 1/2 heterodimers. *J Phys Chem Lett*, 11: 9387-9392. <https://doi.org/10.1021/acs.jpcllett.0c02660>

Google Scholar: [Author Only](#) [Title Only](#) [Author and Title](#)

R Core Team. (2018). R: A Language and Environment for Statistical Computing. R Foundation for Statistical Computing. <https://www.R-project.org>

Google Scholar: [Author Only](#) [Title Only](#) [Author and Title](#)

Raynaud, C., Loiselay, C., Wostrikoff, K., Kuras, R., Girard-Bascou, J., Wollman, F.-A., and Choquet, Y. (2007). Evidence for regulatory function of nucleus-encoded factors on mRNA stabilization and translation in the chloroplast. *Proc Natl Acad Sci USA*, 104: 9093-9098. <https://doi.org/10.1073/pnas.0703162104>

Google Scholar: [Author Only](#) [Title Only](#) [Author and Title](#)

Sambrook, J., and Russell, D. (2001). *Molecular Cloning: A Laboratory Manual* (3 ed.). Cold Spring Harbor Laboratory Press.

Google Scholar: [Author Only](#) [Title Only](#) [Author and Title](#)

Schägger, H., and von Jagow, G. (1991). Blue native electrophoresis for isolation of membrane protein complexes in enzymatically active form. *Anal Biochem*, 199: 223-231. [https://doi.org/10.1016/0003-2697\(91\)90094-A](https://doi.org/10.1016/0003-2697(91)90094-A)

Google Scholar: [Author Only](#) [Title Only](#) [Author and Title](#)

Schneider, A., Steinberger, I., Strissel, H., Kunz, H.-H., Manavski, N., Meurer, J., Burkhard, G., Jarzombski, S., Schünemann, D., Geimer, S., Flügge, U.-I., and Leister, D. (2014). The Arabidopsis Tellurite resistance C protein together with ALB3 is involved in photosystem II protein synthesis. *Plant J*, 78: 344-356. <https://doi.org/10.1111/tpj.12474>

Google Scholar: [Author Only](#) [Title Only](#) [Author and Title](#)

Schult, K., Meierhoff, K., Paradies, S., Toller, T., Wolff, P., and Westhoff, P. (2007). The nuclear-encoded factor HCF173 is involved in the initiation of translation of the psbA mRNA in Arabidopsis thaliana. *Plant Cell*, 19: 1329-1346. <https://doi.org/10.1105/tpc.106.042895>

Google Scholar: [Author Only](#) [Title Only](#) [Author and Title](#)

Sharma, V., Eckels, J., Schilling, B., Ludwig, C., Jaffe, J.D., MacCoss, M.J., and MacLean, B. (2018). Panorama Public: A public repository for quantitative data sets processed in Skyline. *Mol Cell Proteomics*, 17: 1239-1244. <https://doi.org/10.1074/mcp.RA117.000543>

Google Scholar: [Author Only](#) [Title Only](#) [Author and Title](#)

Shimogawara, K., Fujiwara, S., Grossman, A., and Usuda, H. (1998). High-efficiency transformation of Chlamydomonas reinhardtii by electroporation. *Genetics*, 148: 1821-1828. <https://doi.org/10.1093/genetics/148.4.1821>

Google Scholar: [Author Only](#) [Title Only](#) [Author and Title](#)

Somanchi, A., Barnes, D., and Mayfield, S.P. (2005). A nuclear gene of Chlamydomonas reinhardtii, Tba1, encodes a putative oxidoreductase required for translation of the chloroplast psbA mRNA. *Plant J*, 42: 341-352. <https://doi.org/10.1111/j.1365-313X.2005.02378.x>

Google Scholar: [Author Only](#) [Title Only](#) [Author and Title](#)

Spaniol, B., Lang, J., Venn, B., Schake, L., Sommer, F., Mustas, M., Geimer, S., Wollman, F.A., Choquet, Y., Mühlhaus, T., and Schroda, M. (2021). Complexome profiling on the Chlamydomonas lpa2 mutant reveals insights into PSII biogenesis and new PSII associated proteins. *J Exp Bot*. <https://doi.org/10.1093/jxb/erab390>

Google Scholar: [Author Only](#) [Title Only](#) [Author and Title](#)

Staleva, H., Komenda, J., Shukla, M.K., Šlouf, V., Kaňa, R., Polívka, T., and Sobotka, R. (2015). Mechanism of photoprotection in the cyanobacterial ancestor of plant antenna proteins. *Nat Chem Biol*, 11: 287-291. <https://doi.org/10.1038/nchembio.1755>

Google Scholar: [Author Only](#) [Title Only](#) [Author and Title](#)

Suga, M., Ozawa, S.-I., Yoshida-Motomura, K., Akita, F., Miyazaki, N., and Takahashi, Y. (2019). Structure of the green algal photosystem I supercomplex with a decameric light-harvesting complex I. *Nature Plants*, 5: 626-636. <https://doi.org/10.1038/s41477-019-0438-4>

Google Scholar: [Author Only](#) [Title Only](#) [Author and Title](#)

Summer, E.J., Schmid, V., Bruns, B.U., and Schmidt, G.W. (1997). Requirement for the H phosphoprotein in photosystem II of Chlamydomonas reinhardtii. *Plant Physiol*, 113: 1359-1368. <https://doi.org/10.1104/pp.113.4.1359>

Google Scholar: [Author Only](#) [Title Only](#) [Author and Title](#)

Theis, J., and Schroda, M. (2016). Revisiting the photosystem II repair cycle. *Plant Signal Behav*, 11: e1218587-e1218587. <https://doi.org/10.1080/15592324.2016.1218587>

Google Scholar: [Author Only](#) [Title Only](#) [Author and Title](#)

Thompson, J.D., Gibson, T.J., and Higgins, D.G. (2002). Multiple sequence alignment using ClustalW and ClustalX. In *Current Protocols in Bioinformatics*. John Wiley & Sons, Inc. <https://doi.org/10.1002/0471250953.bi0203s00>

Google Scholar: [Author Only](#) [Title Only](#) [Author and Title](#)

Torabi, S., Umate, P., Manavski, N., Plöchinger, M., Kleinknecht, L., Bogireddi, H., Herrmann, R.G., Wanner, G., Schröder, W.P., and Meurer, J. (2014). PsbN is required for assembly of the photosystem II reaction center in Nicotiana tabacum. *Plant Cell*, 26: 1183-1199. <https://doi.org/10.1105/tpc.113.120444>

Google Scholar: [Author Only](#) [Title Only](#) [Author and Title](#)

Trösch, R., Barahimpour, R., Gao, Y., Badillo-Corona, J.A., Gotsmann, V.L., Zimmer, D., Mühlhaus, T., Zoschke, R., and Willmund, F. (2018). Commonalities and differences of chloroplast translation in a green alga and land plants. *Nature Plants*, 4: 564-575. <https://doi.org/10.1038/s41477-018-0211-0>

Google Scholar: [Author Only](#) [Title Only](#) [Author and Title](#)

Tyanova, S., Temu, T., and Cox, J. (2016). The MaxQuant computational platform for mass spectrometry-based shotgun proteomics. *Nat Protoc*, 11: 2301-2319. <https://doi.org/10.1038/nprot.2016.136>

Google Scholar: [Author Only](#) [Title Only](#) [Author and Title](#)

Vaistij, F.E., Boudreau, E., Lemaire, S.D., Goldschmidt-Clermont, M., and Rochaix, J.-D. (2000). Characterization of Mbb1, a nucleus-encoded tetratricopeptide-like repeat protein required for expression of the chloroplast psbB/psbT/psbH gene cluster in *Chlamydomonas reinhardtii*. *Proc Natl Acad Sci USA*, 97: 14813-14818. <https://doi.org/10.1073/pnas.97.26.14813>

Google Scholar: [Author Only](#) [Title Only](#) [Author and Title](#)

van Wijk, K.J. (2015). Protein Maturation and Proteolysis in Plant Plastids, Mitochondria, and Peroxisomes. *Ann Rev Plant Biol*, 66: 75-111. <https://doi.org/10.1146/annurev-arplant-043014-115547>

Google Scholar: [Author Only](#) [Title Only](#) [Author and Title](#)

Walters, R.G., Shephard, F., Rogers, J.J.M., Rolfe, S.A., and Horton, P. (2003). Identification of mutants of *Arabidopsis* defective in acclimation of photosynthesis to the light environment. *Plant Physiol*, 131: 472-481. <https://doi.org/10.1104/pp.015479>

Google Scholar: [Author Only](#) [Title Only](#) [Author and Title](#)

Wang, Q., Sullivan, R.W., Kight, A., Henry, R.L., Huang, J., Jones, A.M., and Korth, K.L. (2004). Deletion of the chloroplast-localized Thylakoid Formation1 gene product in *Arabidopsis* leads to deficient thylakoid formation and variegated leaves. *Plant Physiol*, 136: 3594-3604. <https://doi.org/10.1104/pp.104.049841>

Google Scholar: [Author Only](#) [Title Only](#) [Author and Title](#)

Watkins, K.P., Williams-Carrier, R., Chotewutmontri, P., Friso, G., Teubner, M., Belcher, S., Ruwe, H., Schmitz-Linneweber, C., van Wijk, K.J., and Barkan, A. (2020). Exploring the proteome associated with the mRNA encoding the D1 reaction center protein of Photosystem II in plant chloroplasts. *Plant J*, 102: 369-382. <https://doi.org/10.1111/tbj.14629>

Google Scholar: [Author Only](#) [Title Only](#) [Author and Title](#)

Williams-Carrier, R., Brewster, C., Belcher, S.E., Rojas, M., Chotewutmontri, P., Ljungdahl, S., and Barkan, A. (2019). The *Arabidopsis* pentatricopeptide repeat protein LPE1 and its maize ortholog are required for translation of the chloroplast psbJ RNA. *Plant J*, 99: 56-66. <https://doi.org/10.1111/tbj.14308>

Google Scholar: [Author Only](#) [Title Only](#) [Author and Title](#)

Wollman, F.-A., Minai, L., and Nechushtai, R. (1999). The biogenesis and assembly of photosynthetic proteins in thylakoid membranes. *Biochim Biophys Acta*, 1411: 21-85. [https://doi.org/10.1016/s0005-2728\(99\)00043-2](https://doi.org/10.1016/s0005-2728(99)00043-2)

Google Scholar: [Author Only](#) [Title Only](#) [Author and Title](#)

Xiao, Y., Huang, G., You, X., Zhu, Q., Wang, W., Kuang, T., Han, G., Sui, S.-F., and Shen, J.-R. (2021). Structural insights into cyanobacterial photosystem II intermediates associated with Psb28 and Tsl0063. *Nature Plants*, 7: 1132-1142. <https://doi.org/10.1038/s41477-021-00961-7>

Google Scholar: [Author Only](#) [Title Only](#) [Author and Title](#)

Yohn, C.B., Cohen, A., Danon, A., and Mayfield, S.P. (1996). Altered mRNA binding activity and decreased translational initiation in a nuclear mutant lacking translation of the chloroplast psbA mRNA. *Mol Cell Biol*, 16: 3560-3566. <https://doi.org/10.1128/MCB.16.7.3560>

Google Scholar: [Author Only](#) [Title Only](#) [Author and Title](#)

Zabret, J., Bohn, S., Schuller, S.K., Arnolds, O., Möller, M., Meier-Credo, J., Liauw, P., Chan, A., Tajkhorshid, E., Langer, J.D., Stoll, R., Krieger-Liszka, A., Engel, B.D., Rudack, T., Schuller, J.M., and Nowaczyk, M.M. (2021). Structural insights into photosystem II assembly. *Nature Plants*, 7: 524-538. <https://doi.org/10.1038/s41477-021-00895-0>

Google Scholar: [Author Only](#) [Title Only](#) [Author and Title](#)

Zhan, J., Zhu, X., Zhou, W., Chen, H., He, C., and Wang, Q. (2016). Thf1 interacts with PS I and stabilizes the PS I complex in *Synechococcus* sp. PCC7942. *Mol Microbiol*, 102: 738-751. <https://doi.org/10.1111/mmi.13488>

Google Scholar: [Author Only](#) [Title Only](#) [Author and Title](#)

Zhang, L., Paakkarinen, V., van Wijk, K.J., and Aro, E.-M. (1999). Co-translational assembly of the D1 protein into photosystem II. *J Biol Chem*, 274: 16062-16067. <https://doi.org/10.1074/jbc.274.23.16062>

Google Scholar: [Author Only](#) [Title Only](#) [Author and Title](#)

Zhang, L., Wei, Q., Wu, W., Cheng, Y., Hu, G., Hu, F., Sun, Y., Zhu, Y., Sakamoto, W., and Huang, J. (2009). Activation of the heterotrimeric G protein α -subunit GPA1 suppresses the ftsh-mediated inhibition of chloroplast development in *Arabidopsis*. *Plant J*, 58: 1041-1053. <https://doi.org/10.1111/j.1365-313X.2009.03843.x>

Google Scholar: [Author Only](#) [Title Only](#) [Author and Title](#)

Zimmer, D., Schneider, K., Sommer, F., Schroda, M., and Mühlhaus, T. (2018). Artificial intelligence understands peptide

observability and assists with absolute protein quantification. *Front Plant Sci*, 9. <https://doi.org/10.3389/fpls.2018.01559>

Google Scholar: [Author Only](#) [Title Only](#) [Author and Title](#)

Zoschke, R., and Barkan, A (2015). Genome-wide analysis of thylakoid-bound ribosomes in maize reveals principles of cotranslational targeting to the thylakoid membrane. *Proc Natl Acad Sci USA*, 112: E1678-E1687.

<https://doi.org/10.1073/pnas.1424655112>

Google Scholar: [Author Only](#) [Title Only](#) [Author and Title](#)

Zoschke, R., Chotewutmontri, P., and Barkan, A. (2017). Translation and co-translational membrane engagement of plastid-encoded chlorophyll-binding proteins are not influenced by chlorophyll availability in maize. *Front Plant Sci*, 8.

<https://doi.org/10.3389/fpls.2017.00385>

Google Scholar: [Author Only](#) [Title Only](#) [Author and Title](#)

Zoschke, R., Watkins, K.P., and Barkan, A (2013). A rapid ribosome profiling method elucidates chloroplast ribosome behavior in vivo. *Plant Cell*, 25: 2265-2275. <https://doi.org/10.1105/tpc.113.111567>

Google Scholar: [Author Only](#) [Title Only](#) [Author and Title](#)